A thesis for the degree of Doctor of Philosophy

High-Frequency Acoustic Backscattering

from the Rayleigh Scatterers in Fluid Media

Tae-Hoon Bok

Department of Oceanic Information and System Engineering

GRADUATE SCHOOL

JEJU NATIONAL UNIVERSITY

2011. 8.

High Frequency Acoustic Backscattering from the Rayleigh Scatterers in Fluid Media

Tae-Hoon Bok

(Supervised by professor Dong-Guk Paeng)

A thesis submitted in partial fulfillment of the requirement
for the degree of Doctor of Philosophy

2011. 8.

This thesis has been examined and approved by

Thesis director, Jinho Bae, Associate Professor, Dept. of Ocean System Engineering

----

Chong Hyun Lee, Associate Professor, Dept. of Ocean System Engineering

----

Dong-Guk Paeng, Associate Professor, Dept. of Ocean System Engineering

----

Min Joo Choi, Professor, Dept. of Medicine

Jungyul Na, Emeritus Professor, Hanyang University

2011. 6.

Date

Department of Oceanic Information and System Engineering
GRADUATE SCHOOL
JEJU NATIONAL UNIVERSITY

Dedicated to

Eun Myung Kim

CONTENTS

LIST OF FIGURES

LIST OF TABLES

ABSTRACT

The acoustic backscattering from *Cochlodinium polykrikoides* and red blood cell (RBC) was investigated using high-frequency acoustic measurement systems in the Rayleigh regime. *C. polykrikoides* is a phytoplankton which results in harmful algal blooms in the ocean. RBC is the most abundant cell in blood. The acoustic impedances of two objects are similar with those of corresponding media such as seawater and plasma so that *C. polykrikoides* and RBC are weak scatterers. Hence, high-frequency ultrasound was required for the measurement of backscattering.

The acoustic integrated backscattered power (IBP) from *C. polykrikoides* was measured for 100 s every 15 min during a cultivation of 5 days. The duration of illumination was adjusted daily at 14 h of light and 10 h of darkness. As a result, the IBP was increased overall during the 5-day cultivation, but it was varied daily depending on the duration of illumination. The IBP was increased during light on and was decreased during light off. *C. polykrikoides* reproduces asexually by binary fission and forms a chain so that the IBP is increased overall during cultivation. However, the daily variation cannot be explained by the numerical abundance. It is hypothesized that photosynthesis affects the size of *C. polykrikoides*, because it was reported that the cell volume was increased due to the increase of chlorophyll *a* as the phytoplankton was photosynthesized. However, chlorophyll *a* was no longer produced when the photosynthesis was finished, but was released into the medium

xiv

instead, resulting in the decrease of cell volume. This result expected to be utilized for the physiological research of plankton using acoustics.

Blood echogenicity from whole blood (WB) and RBC suspension was measured at different flow speeds in a mock vessel system with a high-frequency ultrasound biomicroscopy (UBM). For WB, the blood echogenicity was increased as flow speed was decreased because the RBCs aggregated. These phenomena were clarified by the same measurement for RBC suspension. Blood echogenicity was not varied with flow speed for the RBC suspension because the RBC suspension prevents aggregation. Based on these results, blood echogenicity was measured in the radial artery of wrist. The cyclic variation of blood echogenicity was observed in the radial artery. This is because the blood echogenicity was increased and then decreased, resulting in RBC aggregation and disaggregation, respectively, under pulsatile flow, where the flow speed was changed due to the heartbeat. The cyclic variation of blood echogenicity in the radial artery was first observed by ultrasound up to our knowledge. This may contribute to the development of a system for measuring and monitoring blood properties noninvasively *in vivo* using acoustics.

This paper describes the variation of acoustic backscattering from Rayleigh scatterers such as *C. polykrikoides* and RBC. The origins of acoustic backscattering variation were similar, but the mechanisms of biophysical phenomena of the scatterers were different from each other. Consequently, this study can be applied and help advance biological research using acoustics.

Chapter 1

INTRODUCTION

1.1 Background

If an object or inhomogeneity is positioned in the path of a sound wave, it makes the secondary sound spread out from it in various directions. This phenomenon is called scattering of sound. There are many kinds of such objects or inhomogeneities, such as a fish in the ocean, a fog in the air, or a biological tissue in the human body. Among these objects, *Cochlodinium polykrikoides* in the ocean and red blood cell (RBC) in blood are the main targets in this research. Acoustic scattering can play a major role in the measurement of either amount or physical state of these scatterers. In the Rayleigh scattering, in which the acoustic wave length is much larger than the scatterer size, the backscattering is proportional to the fourth power of frequency. In this study, a higher range of frequency in Rayleigh acoustic scattering regime was applied to measure the properties of *C. polykrikoides* and RBC, because both are weak scatterers which need to increase the sensitivity of the backscattering signals.

C. polykrikoides is a phytoplankton which causes harmful algal bloom in the ocean. When it blooms, its abundance is increased and it forms chains, moving along the tidal current in the ocean. They enter the fish body and are collected in the branchia, thereby suffocating the fish. Even though it is not fully understood yet how *C. polykrikoides* is

1

produced and where it comes from, the damage it can cause to fisheries has been recognized. To decrease this damage, it is important to measure the abundance of *C. polykrikoides*. Such abundance can be estimated by the measurement of acoustic scattering from *C. polykrikoides* in the early stage of bloom.

RBC is the most abundant cell in human blood. It delivers oxygen to the body tissues via the blood flow through the circulatory system. Hemoglobin in the RBC carries some of the waste product of carbon dioxide back from the tissues. However, the complexity of the human blood circulation system is not yet fully understood. One of the complexities is RBC aggregation, a condition in which RBCs form a pile, the so-called rouleaux, by electrostatic interactions mediated by macromolecules in the plasma. From the clinical viewpoint, RBC aggregation may play an important role in many diseases such as cardiovascular disease (Hahn *et al.*, 1989; Neumann *et al.*, 1991; Razavian *et al.*, 1992; Resch *et al.*, 1991; Tanahashi *et al.*, 1989), hyperlipidemia (Razavian *et al.*, 1994), malignancies (Khan *et al.*, 1995; Miller and Heilmann, 1989; Sharma *et al.*, 1992), and obesity (Poggi *et al.*, 1994). Hence, the measurement of RBC aggregation is important for the diagnosis of such diseases. Acoustic scattering from blood is the appropriate method to measure RBC aggregation because it is dependent on the abundance of RBCs, the so-called hematocrit, and rouleaux size and distribution.

1.2 Previous studies

Many studies have been accomplished in the field of Rayleigh scattering in acoustics. In this section, the acoustic scatterings are dealt with in the Rayleigh regime with respect to *C. polykrikoides* and RBC.

2.1.1. Acoustic scattering from *Cochlodinium polykrikoides*

C. polykrikoides is a recently appeared species which was first reported by Margalef (Margalef, 1961) and is one of the species through which harmful algal blooms occur. A study of *C. polykrikoides* has attracted researchers since its blooms occurred in the sea around Korea and Japan (Fukuyo *et al.*, 1990; Kim, 1998; Yuki and Yoshimatsu, 1989). However, although biochemical research and optical measurements were mostly investigated, acoustical study was merely accomplished. Recently, acoustical measurements were performed based on the backscattering from *C. polykrikoides* (Bok *et al.*, 2010; Kim *et al.*, 2010). Acoustic scattering from other plankton has also been widely studied. Acoustic volume scattering in the sea at frequencies of 25 kHz–2.5 MHz and 2.5–25 MHz can be explained by the distribution of zooplankton and phytoplankton, respectively (Clay and Medwin, 1977). The physical and acoustical properties of planktons are basic for research, but it is not easy to measure the properties of each species. The physical and acoustical properties were measured for several zooplankton (Greenlaw and Johnson, 1982; Warren and Smith, 2007). The physical and acoustical properties of Antarctic krill (*Euphausia superba*)

were also widely reported (Foote, 1990; Kils, 1979; Køgeler *et al.*, 1987; Morris *et al.*, 1988; Watkins, 1986). Using the acoustic scattering from plankton, the abundance of plankton has been measured for several decades (Chu *et al.*, 1992; Greenlaw, 1979; Greenlaw *et al.*, 1980; Greenlaw and Johnson, 1982; Holliday and Pieper, 1980; Lavery *et al.*, 2007; Lawson *et al.*, 2008; Roberts and Jaffe, 2008; Stanton *et al.*, 1998; Stanton *et al.*, 1994; Wiebe *et al.*, 1996). The acoustic scattering from plankton has been theoretically studied (Anderson, 1950; Machlup, 1952; Stanton, 1988; Stanton, 1989; Stanton *et al.*, 1993; Stanton *et al.*, 1998). However, most of the studies were focused on zooplankton because it has a relatively large size and is a stronger scatterer than phytoplankton. Therefore, the backscattering from phytoplankton, *C. polykrikoides*, was measured and investigated in this research.

2.1.2. Echogenicity from red blood cell

The importance of RBC aggregation was reported in both blood rheology (Knisely, 1965) and blood echogenicity (Cloutier *et al.*, 1996; Shung *et al.*, 1984; Yuan and Shung, 1988). Acoustic scattering from blood was first measured by Shung *et al.* (Shung *et al.*, 1976; Shung *et al.*, 1977), who reported on the angle dependency. Echogenicity, the ability to bounce an echo, is used as a measure of the backscattering properties of tissue (Yuan and Shung, 1989). One review paper with respect to acoustic backscattering from RBC was reported (Cloutier and Qin, 1997b). In the paper, the various influences of experimental factors such as volume of the scatterers, ultrasound frequency, hematocrit, orientation of the

scatterers, flow turbulence, flow pulsatility, and concentration of fibrinogen and dextran were discussed in detail. The shear rate dependence on blood echogenicity was shown by Sigel *et al.* for the first time, and they suggested that increased blood echogenicity *in vitro* results from RBC aggregation (Sigel *et al.*, 1982; Sigel *et al.*, 1983). For the rest, *in vitro* experiments for the relation between the backscattering from RBC and the shear rate were widely reported (Cloutier and Qin, 1997a; Nam *et al.*, 2008; Nam *et al.*, 2009; Paeng *et al.*, 2004a; Paeng *et al.*, 2004b; Paeng *et al.*, 2004c; Razavian *et al.*, 1995a; Razavian *et al.*, 1995b; van der Heiden, Maurits S. *et al.*, 1995). The shear rate dependence on RBC aggregation is shown in Figure 1.1. For *in vivo* measurement, two studies were significantly designed to assess RBC aggregation *in vivo* in humans (Cloutier *et al.*, 1997; Kitamura and Kawasaki, 1997; Li *et al.*, 2011; Paeng and Shung, 2003; Paeng *et al.*, 2010). More *in vivo* studies were also accomplished (Li *et al.*, 2011; Paeng *et al.*, 2010; Rabhi *et al.*, 2002; Wang and Shung, 2001). However, these were performed with low frequency and in large blood vessels.
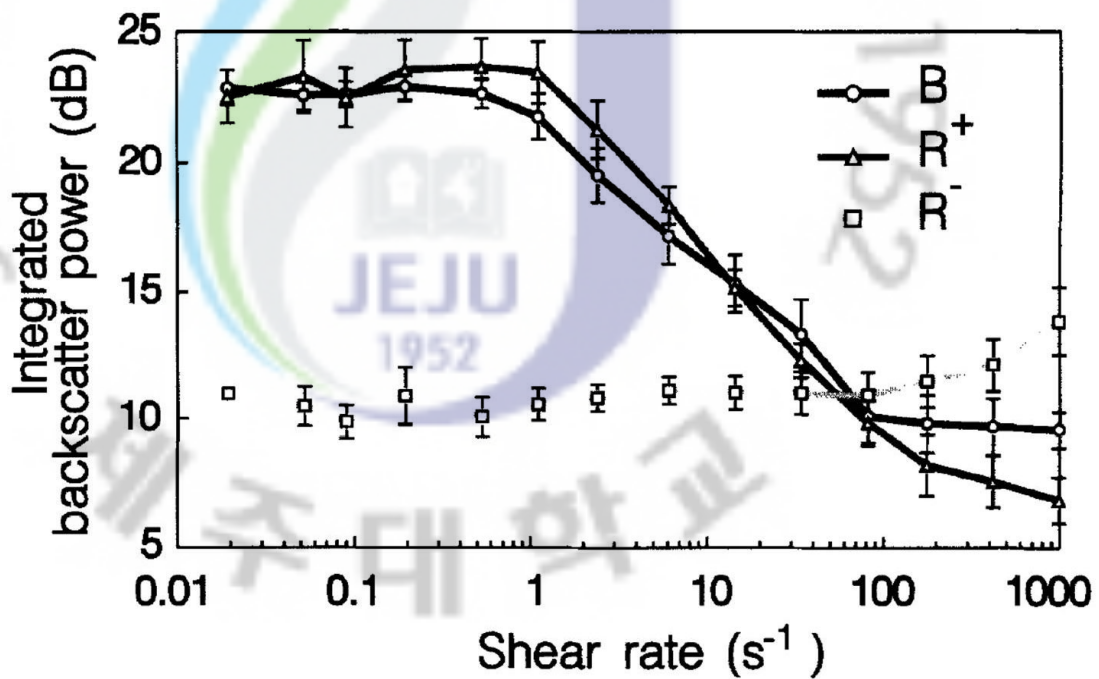
Figure 1.1. Average shear-rate dependency of integrated backscatter power (mean ± standard error of mean) of the three main subsamples: (B) whole blood (n = 6), (R[+]) rouleaux-enhanced blood (n = 3 of 6) and (R[-]) rouleaux-suppressed blood (n = 3 of 6) (van der Heiden, Maurits S. *et al.*, 1995).

1.3 Specific aims

The objectives of the present research are to measure acoustic backscattering from Rayleigh scatterers such as *C. polykrikoides* and RBC, and to interpret the backscattering variations. To accomplish these objectives, the aims of this research are subdivided into three as follows.

The first aim is to study the acoustic backscattering from *C. polykrikoides*. In previous studies, acoustical approaches to measure the abundance of *C. polykrikoides* have been rarely accomplished even though damages due to harmful algal blooms of *C. polykrikoides* are increasing. To investigate the backscattering from *C. polykrikoides*, acoustic backscattered signals were acquired during the five-day cultivation of *C. polykrikoides*. The variations of acoustic backscattering were obtained and were interpreted by Rayleigh scattering with the physiological phenomena of *C. polykrikoides*.

The second aim is to apply Rayleigh scattering to RBC using high-frequency ultrasound. Blood echogenicity has long been studied with respect to RBC aggregation but mainly at low frequency. In this study, the high-frequency application to RBC aggregation was performed under the Rayleigh regime. To investigate the acoustic backscattering from RBC, the steady flow was generated in the mock blood vessel system, and the ultrasound B-mode images were acquired depending on the flow speed for porcine whole blood (WB) and RBC suspension. Results confirmed that the increasing blood echogenicity was due to RBC aggregation at low flow speed and low shear rate.

The last aim is to *in vivo* measure the acoustic backscattering from blood in the radial artery at the wrist. A study measuring acoustic signals in the radial artery in order to investigate RBC aggregation *in vivo* has not been reported yet. The acoustic signal is mostly measured in large arteries such as a common carotid artery. To study the acoustic scattering from RBC in the radial artery, ultrasound B-mode images were acquired for several seconds using high-frequency UBM. The cyclic variation of blood echogenicity was observed in the radial artery.

1.4 Thesis outline

Chapter 2 provides background knowledge for this study including the acoustical properties of scatterers such as RBC and *C. polykrikoides*, and the acoustic scattering in Rayleigh regime.

Chapter 3 shows the experimental results of the integrated backscattered power (IBP) from *C. polykrikoides* during cultivation. This experiment presents that the IBP can be periodically varied depending on the growth of *C. polykrikoides*.

Chapter 4 presents the experimental results of echogenicity from aggregating porcine WB and non-aggregating RBC suspensions as a function of flow speed under steady flow in a mock flow loop. This experiment aims to investigate the principle of variation in blood echogenicity measured by high-frequency UBM.

Chapter 5 reports the experimental results of blood echogenicity in the radial artery

using UBM. This is the first measurement of cyclic variation of blood echogenicity in the

radial artery, especially with an ultrasound B-mode image in the field of ultrasound blood

imaging.

Chapter 6 concludes this study and suggests future directions for research.

Chapter 2

BACKGROUND KNOWLEDGE

2.1 Acoustic scattering in Rayleigh regime

2.1.1. Basic concept of scattering

When an acoustic wave propagates, it can meet an object and be reflected or scattered from the object. The shape of an object is sometimes considered to be a sphere in order to simplify the acoustical phenomena with some assumptions and approximations. Nevertheless, scattering from a sphere has been widely studied due to its simplicity. A dominant feature of scattering phenomena is mainly focused on low-frequency scattering. Low-frequency scattering compared to the scatterer size is often referred to as Rayleigh scattering because Rayleigh had contributed to developing the basic theory (Rayleigh, 1897; Rayleigh, 1972).

2.1.2. Scattering function

The relation among the intensity of incident plane wave (I_p), the scattered sound intensity (I_s), and the distance to the receiver (R) is written as

$$I_s \sim \frac{I_p}{R^2} \ . \tag{2.1}$$

At long range, $I_p = P_p^2 / (\rho_A c)$ and $I_s = P_s^2 / (\rho_A c)$, (2.1) can be written as

$$P_s^2 \sim \frac{P_p^2}{R^2} \quad , \tag{2.2}$$

where P_p and P_s are the corresponding pressures of the incident and the scattered sound, and ρ_A and c are the density and the sound speed of the medium, respectively. The constants of proportionality depend on the frequency of sound, as well as the size, shape, and orientation of the object with respect to the source and the receiver (Clay and Medwin, 1977). This is described by

$$I_s = \frac{I_p}{R^2} \zeta(\theta, \varphi, \theta_p, \varphi_p, f) \, A(\theta_p, \varphi_p) \quad , \tag{2.3}$$

where ζ is the scattering function of $\theta, \varphi, \theta_p, \varphi_p$ and f. A is the cross section of the projected area of the scatterer viewed from the source. ζ is often a very complicated function of angles as well as the frequency and the dimensions of the object. θ, φ and θ_p, φ_p are the spherical coordinates of the scattered and the incident sound, respectively. f is the frequency of sound. For simplicity and practicality, two cases are dealt with, such as the backscattered sound $\theta = 180°$ ($\varphi = 0°$) and the total scattered sound.

2.1.3. Rayleigh scattering

When the sound wavelength (λ) is greater than the spherical scatterer, it is defined as Rayleigh scattering and is described by

$$2\pi a \ll \lambda \quad \rightarrow \quad \frac{2\pi}{\lambda} a \ll 1 \quad \rightarrow \quad ka \ll 1 \quad , \tag{2.4}$$

where a = radius of sphere, and k = wave number.

11

The scattering function for a small non-resonant sphere is expressed by

$$\zeta = \frac{(ka)^4}{\pi}\left[\frac{gh^2-1}{3gh^2} - \frac{g-1}{2g+1}\cos\theta\right]^2 \ ,$$

(2.5)

where g and h are the density ratio and the sound speed ratio between the sphere and the medium, respectively, and θ is the angle between the incident and scattered direction (Clay and Medwin, 1977). Equation (2.5) was derived for a sphere, but it has been shown that non-spherical effects can usually be ignored when scattering is in the Rayleigh region (Palmer, 1996). The backscattering function, $\zeta_{bs,}$ is obtained by setting $\theta=180°$.

The total backscattering cross section σ_{bs} is determined by integrating over the range of possible orientations. It is described by

$$\sigma_{bs} = \pi a^2 \int_0^{4\pi} \zeta_{bs}\ d\Omega = 4\pi a^2 (ka)^4\left[\left(\frac{gh^2-1}{3gh^2}\right)^2 + \left(\frac{g-1}{2g+1}\right)^2\right] \ .$$

(2.6)

The backscattering strength S_b is the logarithm of Equation (2.6), which is expressed as

$$S_b \ = \ 10\log_{10}\sigma_{bs} \ ,$$

(2.7)

and the volume backscattering strength S_v is given by

$$S_v \ = \ 10\log_{10}\left(\sigma_{bs}N\right) \ ,$$

(2.8)

where N is the numerical abundance of scatterers.

Multiple scattering is assumed to be ignored. *C. polykrikoides* exists as an individual cell initially, where the backscattering cross section can be multiplied by the numerical abundance to obtain the volume scattering strength. However, it usually forms a chain by binary fission during growth. It is not simple to accurately compute the backscattering from those chains. A

12

chain with less than six cells is smaller than a wavelength of 5 MHz, so that each chain

scatterer with less than six cells is assumed to be a Rayleigh scatterer of a compressible sphere

with equivalent volume. For volume scattering, the backscattering cross section of a Rayleigh

scatterer with equivalent volume is multiplied by the number of chains. Similarly, RBCs form

piles called rouleaux. Rouleaux are also considered as a size-increased scatterer, so it is not

easy to theoretically calculate the backscattering from rouleaux. Hence, rouleaux are also

assumed to be a Rayleigh scatterer with equivalent volume, and volume scattering can be

computed by multiplying the backscattering cross section and the number of rouleaux.

If g, h, a, and N are given, then the theoretical value of S_v can be easily estimated using

Equation (2.8). However, it is difficult to obtain the values of g and h of a plankton, thus

making it difficult to compute the theoretical S_v. It is much easier to compute the IBP instead

of estimating the quantitative value of S_v. The IBP is proportional to S_v if the same transducer

is used in the same electronic system. The acoustic IBP is defined by

$$\text{IBP} = 20\log_{10}\left(\frac{V_{\text{rms, bs}}}{V_{\text{rms, ref}}}\right) \ , \tag{2.9}$$

where $V_{\text{rms, bs}}$ and $V_{\text{rms, ref}}$ are the root mean squared voltages of the backscattered signal from

a scatterer and a reference, respectively. The IBP was computed for analysis of the acoustical

data obtained from *C. polykrikoides*. The beam pattern signal was used as the reference data

$V_{\text{rms, ref}}$ in Equation (2.9) (Bok *et al.*, 2010).

13

2.2 Properties of *Cochlodinium polykrikoides* and red blood cell

2.2.1. *Cochlodinium polykrikoides*

C. polykrikoides, which was first reported from the Caribbean Sea along the southern coast of Puerto Rico (Margalef, 1961), is an unarmored, marine, planktonic dinoflagellate and photosynthetic species shaped like a spiral cingulum. It produces common harmful algal blooms in Korea and Japan (Fukuyo *et al.*, 1990; Kim, 1998; Yuki and Yoshimatsu, 1989). Size, density, and sound speed of the scatterer are very important in computing acoustic scattering for Rayleigh scattering. The size of the *C. polykrikoides* cell is in the range of 30–40 μm in length and 20–30 μm in width, as shown in Figure 2.1 (Fukuyo *et al.*, 1990; Silva, 1967; Steidinger and Tangen, 1996; Taylor *et al.*, 1995). The density of *C. polykrikoides* has not been reported yet. Very accurate and precise experiments are needed to measure the density of phytoplankton, making it difficult to measure the density accurately. The density of *C. polykrikoides* would be analogized to 1.078 g/cm^3 as the average by the previous reported data for other dinoflagellate (Kamykowski *et al.*, 1992) as shown in Table 2.1. To date, the sound speed of phytoplankton has been rarely studied. The sound speed of *Skeletonema costatum*, a diatom, has been estimated as 1,530 m/s based on the relation between compressional wave velocity and density (Blanc *et al.*, 2000).

C. polykrikoides reproduces asexually by binary fission, and its plane of fission is oblique (Silva, 1967) and forms a chain (Jiang *et al.*, 2010; Matsuoka *et al.*, 2008). The

14

number of cells is rapidly increased under certain conditions and harmful algal bloom occurs

in the ocean (Gárate-Lizárraga *et al.*, 2004; Mulholland *et al.*, 2009; Yamasaki *et al.*, 2007).

This is an interesting characteristic in the acoustic measurement because the number of

scatterers and the size of one scatterer are both increased.
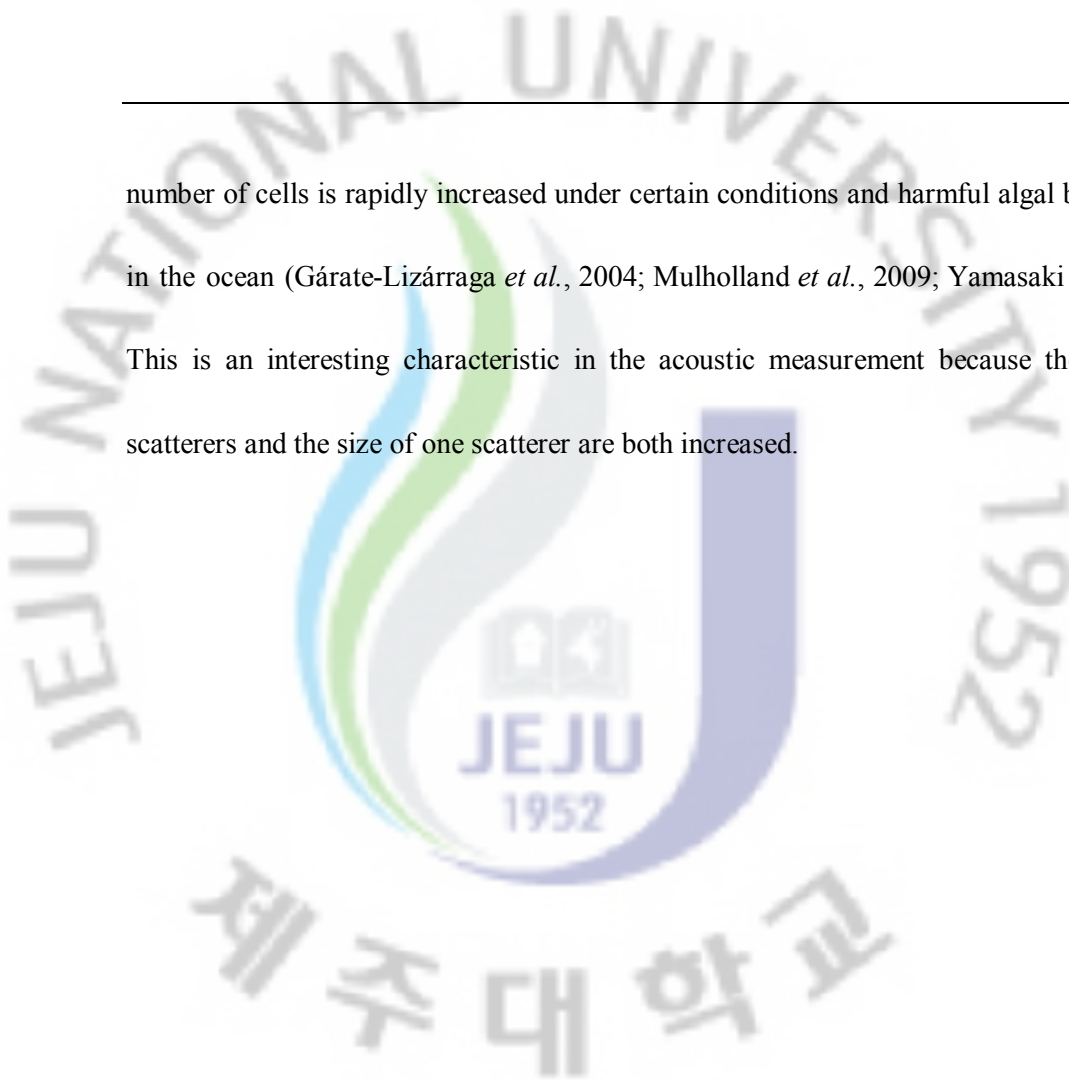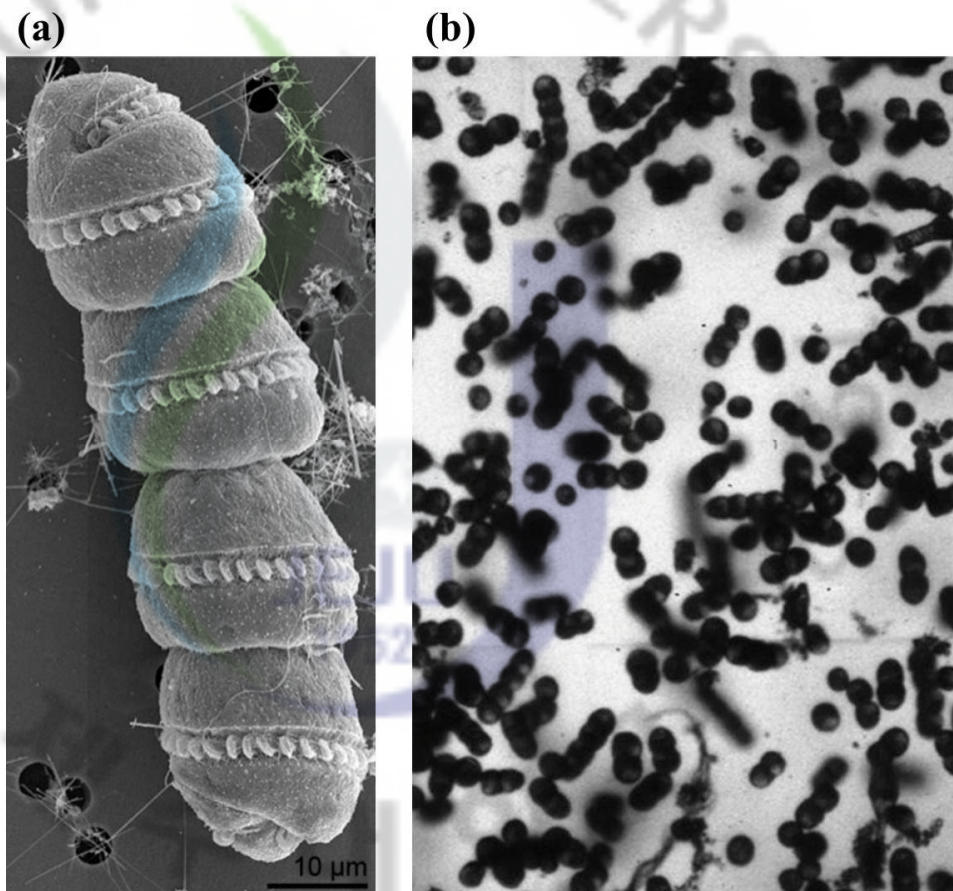
Figure 2.1. Photograph of four cell-chained *Cochlodinium polykrikoides* (a) (Hansen, 2011) and a group of *C. polykrikoides* (b) (Matsuoka and Fukuyo, 2011).

Table 2.1. Densities of several dinoflagellates (Kamykowski *et al.*, 1992)

Species	Density (g/cm^3)
Prorocentrum mariae-lebouriae	1.064 ± 0.015
Scrippsiella trochoidea	1.077 ± 0.007
Peridinium foliaceum	1.080 ± 0.012
Gymnodinium sanguineum	1.073 ± 0.007
Gyrodinium dorsum	1.090 ± 0.009
Gonyaulax polyedra	1.084 ± 0.007

2.2.2. Red blood cell

Blood is a bodily fluid comprised of RBC, white blood cell, and platelet suspended in a liquid called plasma. Plasma constitutes 55% of blood and is mostly water. Among the other components, except for plasma in blood, RBCs are the most abundant cells in vertebrates. Blood properties such as cell number, size, protein structure, and so on are somewhat dependent on the species (Romer and Parsons, 1977), but human blood is the target of this study. Human RBC is shaped like a biconcave disc approximately 8 μm in diameter and about 2 μm thick, as shown in Figure 2.2(a). The density of plasma is approximately 1,025 kg/m^3 and the density of blood cells is approximately 1,125 kg/m^3 (Benson, 1999).

RBCs aggregate to form rouleaux under normal physiological conditions in plasma, as shown in Figure 2.2(b). This is an interesting phenomenon in hemorheology because RBC aggregation affects the flow dynamics and flow resistance of blood. However, the pathophysiological effects of RBC aggregation have not been fully studied yet. The mechanism to form rouleaux is very complicated and is not yet well understood. Briefly, two models were proposed to explain RBC aggregation, namely, the bridging model and the depletion model (Armstrong *et al.*, 1999; Baumler *et al.*, 1999; Brooks *et al.*, 1980; Donath *et al.*, 1993; Evans *et al.*, 1991; Rampling *et al.*, 2004; van Oss *et al.*, 1990). These are very important phenomena in acoustic scattering because RBC aggregation forming rouleaux increases the scatterer size.

17
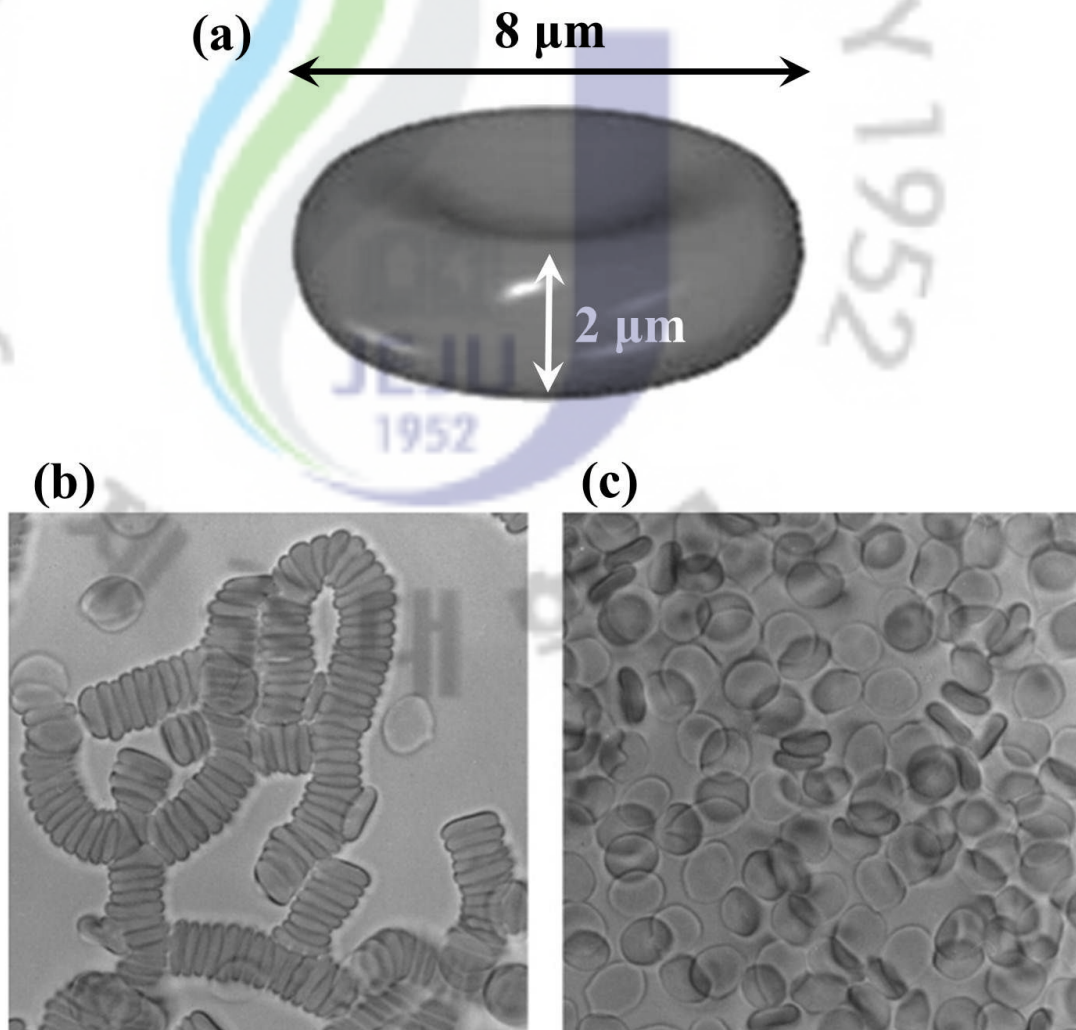
Figure 2.2. Conceptual picture of red blood cell (a) and microscopic photograph of blood: human red blood cells in plasma (b) and in saline (c). Magnification ×400 (Fatkin *et al.*, 1997).

Chapter 3

HIGH-FREQUENCY ACOUSTIC BACKSCATTERING FROM

COCHLODINIUM POLYKRIKOIDES

3.1 Introduction

C. polykrikoides is the main species of harmful algal bloom in Korean seawater and becomes dominant in seawater during harmful algal bloom (Yoo *et al.*, 1999). To observe harmful algal bloom of *C. polykrikoides* in the sea, many studies have been performed using advanced very high-resolution radiometer (AVHRR) sensor in satellites (Ahn *et al.*, 2005; Suh *et al.*, 2000). However, this sensor is limited by weather conditions and technical problems, such that the AVHHR can only observe the physical and chemical changes in near-surface seawater after a bloom. Recently, acoustic backscattering measurements were suggested to observe harmful algal bloom (Bok *et al.*, 2010; Kim *et al.*, 2010). They acquired the acoustic backscattered power from *C. polykrikoides* to observe the harmful algal bloom of *C. polykrikoides* in the ocean *in situ*.

According to Equations 2.6, 2.8, and 2.9, the IBP is proportional to the volume scattering strength, which is the function of the wave number (k), the scatterer size (a), the density ratio (g), the sound speed ratio (h), and the abundance of scatterers (N). N is related to harmful algal bloom so that the experimental study with respect to the relation between IBP and N could be accomplished. In this chapter, the IBP was measured at several

19

numerical abundances during cultivation of *C. polykrikoides*. The IBP at different numerical

abundances was measured to understand the backscattered power depending on the number

of the scatterers. During cultivation of *C. polykrikoides*, the IBP was observed to investigate

whether it varies or not, and how and why it varies if it does.

3.2 Methods and materials

3.2.1. Cultivation of *Cochlodinium polykrikoides*

There were two kinds of cultivations. The first cultivation was to monitor the growth

rate of *C. polykrikoides*. The second cultivation was conducted simultaneously measuring the

acoustic signal To culture *C. polykrikoides* in the laboratory, the methods of Guillard and

Ryther (Guillard and Ryther, 1962) and Guillard (Guillard, 1975) were followed, as shown in

Table 3.1. Seawater from the Southern Sea of Korea (with approximately 33 psu salinity)

was filtered with 0.45 mm glass filter paper, placed in a 10 L bottle (Nalgene, Rochester, NY,

USA), and autoclaved. The chemical compounds were added, and the media were autoclaved

again and kept at room temperature for 24 h. For these processes, an f/2 medium was

prepared with autoclaved enriched seawater (Guillard and Ryther, 1962). An inoculum of *C.*

polykrikoides was added to a 600 ml cell culture flask (Corning Inc., Corning, NY, USA) for

an initial culture of 100 cell/ml. The inoculums (*C. polykrikoides* strain BWE0109) were

obtained from the Biocenter at the Polar Applied Science Division of the Korea Polar

Research Institute. The culture was maintained in an incubator at 23–24 °C under 2500 lx

fluorescent illumination for a light-to-dark cycle of 14–10 h (Lee *et al.*, 2001). The number of cells was counted frequently using a microscope (DW-THN, Dongwon Systems Corporation, Seoul, Korea). After pipetting 100 ml samples of the culture medium into a counting plate (96-well Cell Culture Cluster, Corning Inc., Corning, NY, USA), the samples were fixed in a Lugol's iodine solution. The number of cells was counted with a magnification factor of ×150. Counting was done in triplicate and cell numbers were averaged.

Table 3.1. The compounds of f/2 medium (a), f/2 trace metal solution (b), and f/2 vitamin solution (c) by Guillard and Ryther (Guillard and Ryther, 1962) and Guillard (Guillard, 1975) methods.

(a) f/2 medium, to 950 ml filtered seawater add:

Quantity	Compound	Stock Solution	Molar Concentration in Final Medium
1 ml	$NaNO_3$	75 g/L dH_2O*	8.83×10^{-4} M
1 ml	$NaH_2PO_4 \cdot H_2O$	5 g/L dH_2O	3.63×10^{-5} M
1 ml	$Na_2SiO_3 \cdot 9H_2O$	30 g/L dH_2O	1.07×10^{-4} M
1 ml	f/2 trace metal solution	(b)	
0.5 ml	f/2 vitamin solution	(c)	

Make final volume up to 1 L with filtered seawater.

(b) f/2 trace metal solution, to 950 ml dH_2O add:

Quantity	Compound	Stock Solution	Molar Concentration in Final Medium
3.15 g	$FeCl_3 \cdot 6H_2O$		1×10^{-5} M
4.36 g	$Na_2EDTA \cdot 2H_2O$		1×10^{-5} M
1 ml	$CuSO_4 \cdot 5H_2O$	9.8 g/L dH_2O	4×10^{-8} M
1 ml	$Na_2MoO_4 \cdot 2H_2O$	6.3 g/L dH_2O	3×10^{-8} M
1 ml	$ZnSO_4 \cdot 7H_2O$	22.0 g/L dH_2O	8×10^{-8} M

Make final volume up to 1 L with dH_2O.

(c) f/2 vitamin solution, to 950 ml dH_2O add:

Quantity	Compound	Stock solution	Molar Concentration in Final Medium
1 ml	Vitamin B_{12} (cyanocobalamin)	1.0 g/L dH_2O	1×10^{-10} M
10 ml	Biotin	0.1 g/L dH_2O	2×10^{-9} M
200 mg	Thiamine $\cdot$ HCl		3×10^{-7} M

Make final volume up to 1 L with dH_2O.

* dH_2O is distilled water.

3.2.2. High-frequency acoustic measurement system

The experimental setup is schematically shown in Figure 3.1 and the parameters are presented in Table 3.1. To maintain a uniform distribution of *C. polykrikoides* in the cultured media, a spin ball was placed and rotated by a magnetic stirrer at the bottom of the water tank (with an inner radius of 5 cm and a height of 15 cm). A transducer (A308, Panametrics, USA) with 19 mm diameter aperture at a central frequency of 5 MHz was connected to a pulser/receiver (500PR, Panametrics, USA) which generated the pulses and received the backscattered signals from the cultured media with *C. polykrikoides*. The parameters of the pulser/receiver were as follows: damping was 5, gain was 8, and pulse repetition frequency was 500 Hz. Pulse length was 0.4 μs. A digital oscilloscope (LT322, LeCroy, USA) was used for data acquisition and display of the generated and backscattered signals, which were transferred to a personal computer for further processing (Bok *et al.*, 2010).
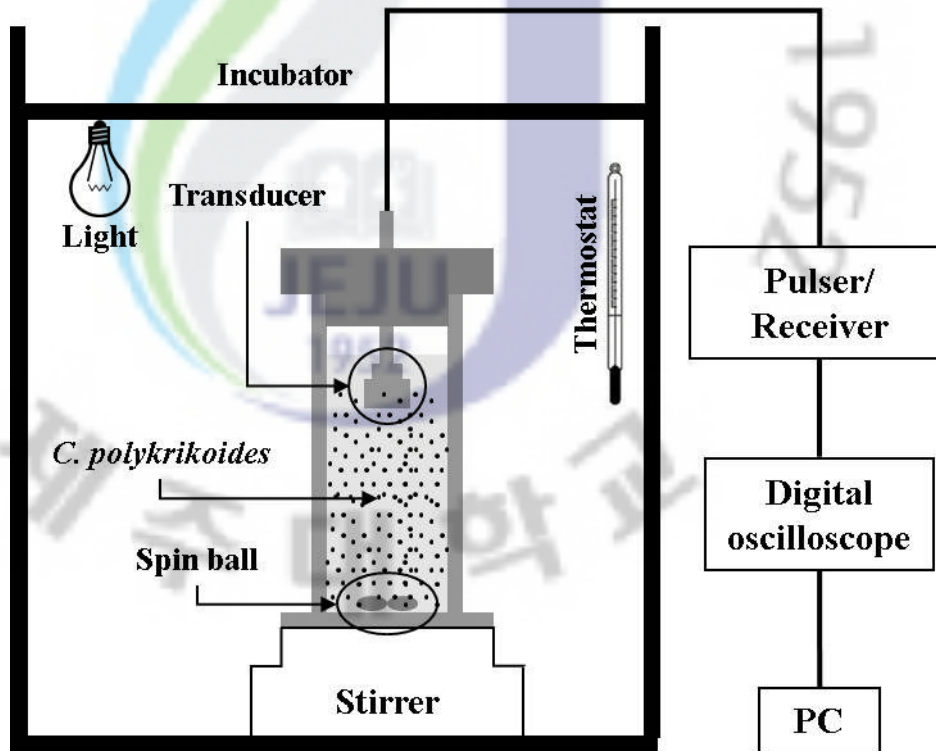
Figure 3.1. Experiment setup for measurement of the backscattered power from *Cochlodinium polykrikoides* during cultivation.

3.2.3. Data acquisition

3.2.3.1. Acoustic signal acquisition at different numerical abundance of *C. polykrikoides*

According to the warning system of harmful algal bloom in Korea, precaution and warning levels are above 300 and 1,000 cell/ml, respectively. Thus, the numerical abundance of *C. polykrikoides* was adjusted to 90, 110, 200, 260, 300, 340, 360, 600, 700, and 850 cell/ml in order to measure the acoustic IBP before harmful algal bloom warning. The backscattered signals from *C. polykrikoides* media and the beam profile data were used as $V_{rms, bs}$ and $V_{rms, ref}$, respectively, in Equation (2.9). Twenty signals were acquired at each amount. Average and standard deviations of the IBP were calculated from 20 signals for each amount.

3.2.3.2. Acoustic signal acquisition during cultivation

The initial numerical abundance of *C. polykrikoides* was 100 cell/ml. A total of 100 signals were acquired for 100 s per 15 min. Data acquisition was maintained for five days during cultivation. The light was automatically turned on and off—light on for 14 h and off for 10 h. The other factors were not changed during cultivation. Average and standard deviations of the IBP were calculated from 100 signals for each measurement time.

3.3 Results

3.3.1. Acoustic integrated backscattered power from *Cochlodinium polykrikoides*

Backscattered signals were obtained for the 10 different values of numerical abundance at 5 MHz. The presence of *C. polykrikoides* and the increase of numerical abundance resulted in an increase in the amplitude of backscattered signals. Figure 3.2 shows the IBP versus the numerical abundance of *C. polykrikoides* at 5 MHz. The circles are the IBP values averaged over 20 pings corresponding to the numerical abundance of *C. polykrikoides* at 5 MHz, and the standard deviation limits are shown as error bars. The solid line is a curve fit to the IBP. The curve-fitted IBP values were about -28 dB *ref. $V_{rms,\ fresh\ water}$* and -23 dB *ref. $V_{rms,\ fresh\ water}$* with the density of 300 and 850 cell/ml, respectively (Bok *et al.*, 2010).
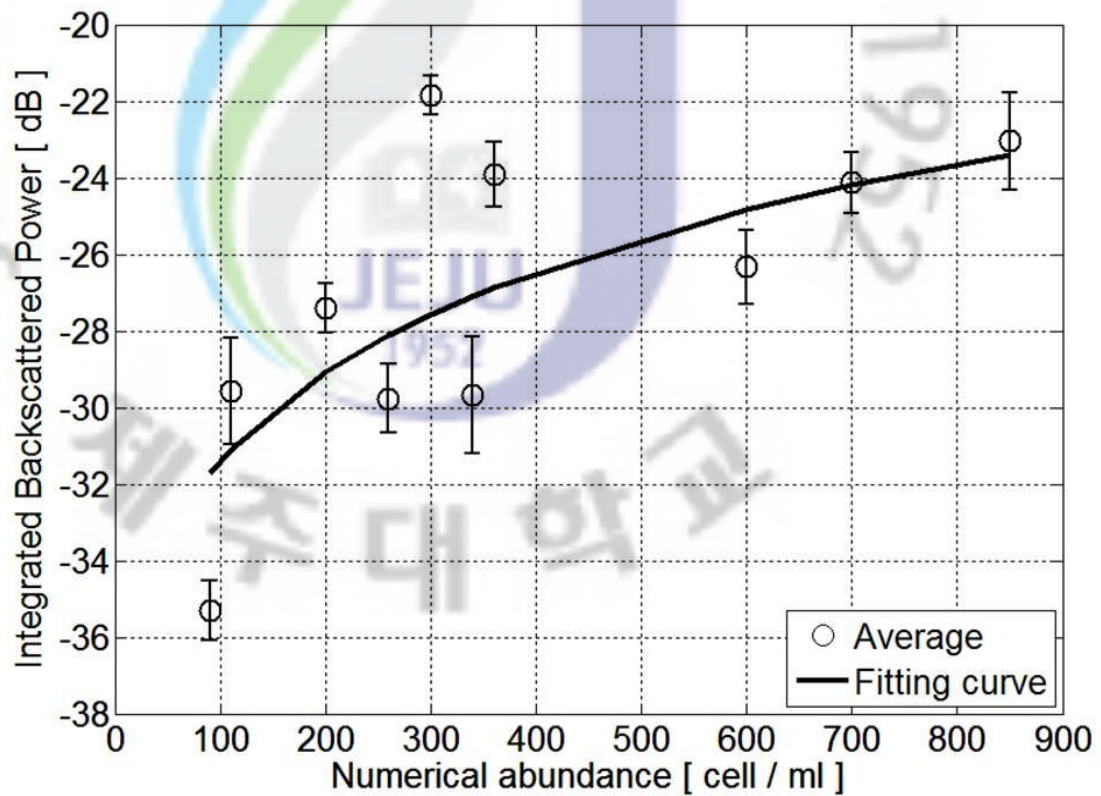
Figure 3.2. Integrated backscattered power from *Cochlodinium polykrikoides* as a function of the numerical abundance at 5 MHz. The unit of decibel is dB *ref. V_{rms, fresh water}* (Bok *et al.*, 2010).

3.3.2. Growth rate of *Cochlodinium polykrikoides* during cultivation

Figure 3.3 indicates the growth rate of *C. polykrikoides* during the first cultivation. Numerical abundance was gradually increased up to 274 ± 40 cell/ml on the 8th day and then rapidly increased up to $1,784 \pm 48$ cell/ml on the 29th day. Thereafter, numerical abundance was decreased. Error bars indicate the standard deviation in numerical abundance for three different culturing bottles (Bok *et al.*, 2010).
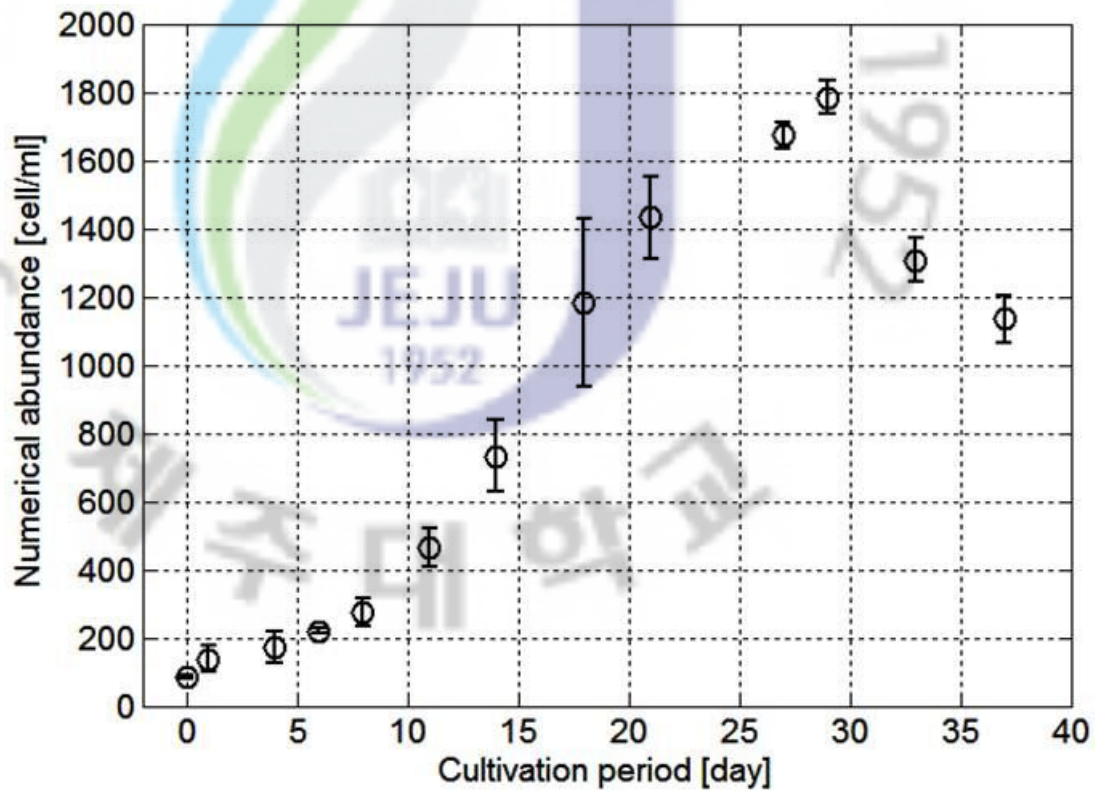
Figure 3.3. Growth rate of *Cochlodinium polykrikoides* showing the increase and decrease of numerical abundance during cultivation. Error bars indicate the standard deviation in the numbers of cells for three different culturing bottles (Bok *et al.*, 2010).

3.3.3. Daily variation of acoustic integrated backscattered power

The acoustic IBP from culturing media of *C. polykrikoides* was periodically varied during the second cultivation (Figure 3.4). When the cultivation started, the light was turned on for 14 h. Initially, the IBP was increased from -32 dB *ref. $V_{rms,\ fresh\ water}$* to -31 dB *ref. $V_{rms,\ fresh\ water}$* until the light was off. However, the IBP was decreased after the light was turned off for 10 h. The decrease was kept from -31 dB *ref. $V_{rms,\ fresh\ water}$* to -32 dB *ref. $V_{rms,\ fresh\ water}$* until the light was turned on. The phenomena of increase and decrease were repeated during cultivation. The IBP was increased for five days. Initial IBP was -32 dB *ref. $V_{rms,\ fresh\ water}$* and final IBP was -31 dB *ref. $V_{rms,\ fresh\ water}$* in five days.
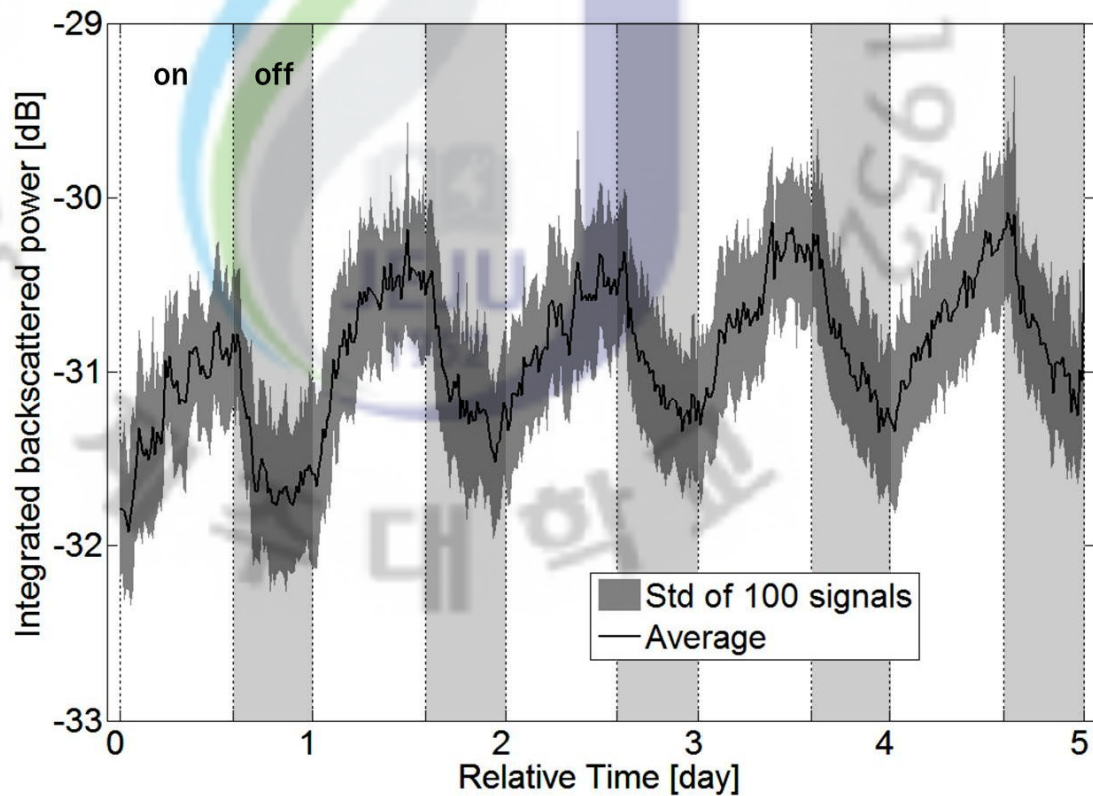
Figure 3.4. Variation of integrated backscattered power from *Cochlodinium polykrikoides* during cultivation at 5 MHz. The unit of decibel is dB *ref. V$_{rms, fresh water}$*.

3.4 Discussion

The IBP from *C. polykrikoides* was increased as the numerical abundance of *C. polykrikoides* was increased. This is well explained by the relation between the backscattered power and the number of scatterers. The backscattered power is proportional to the volume backscattering strength and to the number of scatterers. Therefore, the acoustic backscattered power is increased as the number of scatterers is increased (Figure 3.2). During cultivation, on the other hand, the sequential acquisition of acoustic signal shows different results (Figure 3.4). The backscattered power from *C. polykrikoides* increased when the light was turned on and decreased when the light was turned off. This is not simply explained by the relation between the backscattered power and the number of scatterers. There are two possible explanations for this as follows.

3.4.1. Growth of *Cochlodinium polykrikoides*

Although acoustic signals were acquired during the second cultivation, it took five days from the initial time to the end of measurement of acoustic signals (Figure 3.4). According to the growth rate of *C. polykrikoides,* numerical abundance was increased up to approximately 200 cell/ml for the first five days (Figure 3.3). However, the numerical abundance could not be counted during the second cultivation with the measurement of acoustic signals because of the stability of measurement setup. Nevertheless, we can estimate how much the numerical abundance was increased using the acoustic scattering theory. In Chapter 3.3.1,

32

backscattered power was measured depending on the numerical abundance (Figure 3.2). According to the fitting curve, the IBP was approximately -31.5 dB *ref. V$_{rms, fresh water}$* at 100 cell/ml and -29 dB *ref. V$_{rms, fresh water}$* at 200 cell/ml. The fitting curve was also represented by matching both of the y-axes in Figure 3.5. Theoretically, if the number of scatterers doubles, the IBP increases as 3 dB. However, the IBP was increased as 2.5 dB in the fitting curve. In Figure 3.3, the numerical abundance values were 84 ± 5, 138 ± 37, and 170 ± 46 cell/ml at the first three measurements, respectively. The averages of the three values are represented as x-marks in Figure 3.5. This means that -32 dB *V$_{rms, fresh water}$* could be estimated by 84 ± 5 cell/ml, -30.6 dB *ref. V$_{rms, fresh water}$* by 138 ± 37 cell/ml, and -29.3 dB *ref. V$_{rms, fresh water}$* by 170 ± 46 cell/ml.

In this chapter, there were two cultivations. The first cultivation was performed for more than 30 days with the numerical abundance counting but the acoustic backscattered power not measured (Figure 3.3). The second cultivation was performed for five days without the numerical abundance counted but the acoustic backscattered power measured (Figure 3.4). Moreover, the acoustic measurement was accomplished with the arbitrary numerical abundance values counted (Figure 3.2). With this result, the fitting curve between the IBP and the numerical abundance can be divided by two y-axes, such as the left y-axis for the IBP and the right y-axis for the numerical abundance. Each axis is numerically matched in Figure 3.5. The IBP could also be estimated by the numerical abundance in the first cultivation, and the numerical abundance could be estimated by the IBP in the second cultivation. In this way, two results should be theoretically the same; however, such was not the case. The increasing

pattern for the three x-marks from the first cultivation was not followed in the second cultivation. This is possibly caused by the different cultivation environmental conditions, such as the healthy condition of *C. polykrikoides*, the chain-forming ability, and so on.

On one hand, the daily variation of increasing and decreasing pattern cannot be explained by the numerical abundance. This is assumed as the daily variation caused by the photosynthesis effect. This is explained in the next section.
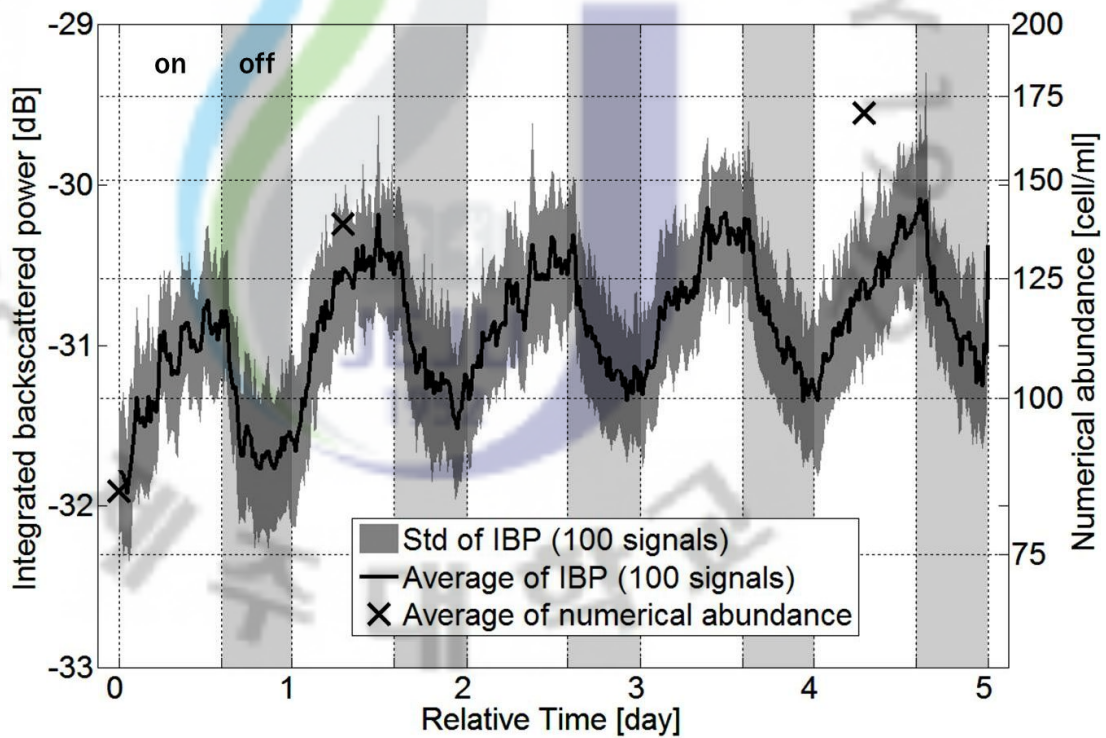
Figure 3.5. Variation of integrated backscattered power from *Cochlodinium polykrikoides* at 5 MHz and growth rate of the numerical abundance during cultivation. The unit of decibel is dB *ref. V*_{rms, fresh water}. The left y-axis corresponds to the right y-axis by the fitting curve of Figure 3.2. The three x-marks correspond to the averages of the numerical abundance in Figure 3.3.

3.4.2. Assumption: Photosynthesis effect on *Cochlodinium polykrikoides*

When the acoustic signal was measured during cultivation, light was the only variable factor. The light was turned on for 14 h and off for 10 h periodically to simulate the actual period of light in a day. In this case, *C. polykrikoides* photosynthesizes. In general, many studies about the photosynthesis of phytoplankton have been reported (Lewitus and Kana, 1994; Oh *et al.*, 2006). Marañón *et al.* reported the relation between photosynthesis and phytoplankton cell size (Marañón *et al.*, 2007). As phytoplankton photosynthesizes, both the amount of chlorophyll *a* and the cell volume are increased (Figure 3.6). Therefore, we can assume that the volume of a scatterer, *C. polykrikoides*, is increased so that the backscattered power can be increased during photosynthesis. Furthermore, *C. polykrikoides* does not photosynthesize during the dark period, so chlorophyll *a* is not produced in the cell but is released into the medium instead, decreasing the cell volume. To verify this hypothesis, chlorophyll *a* should be measured while the backscattered power is measured during cultivation.

36
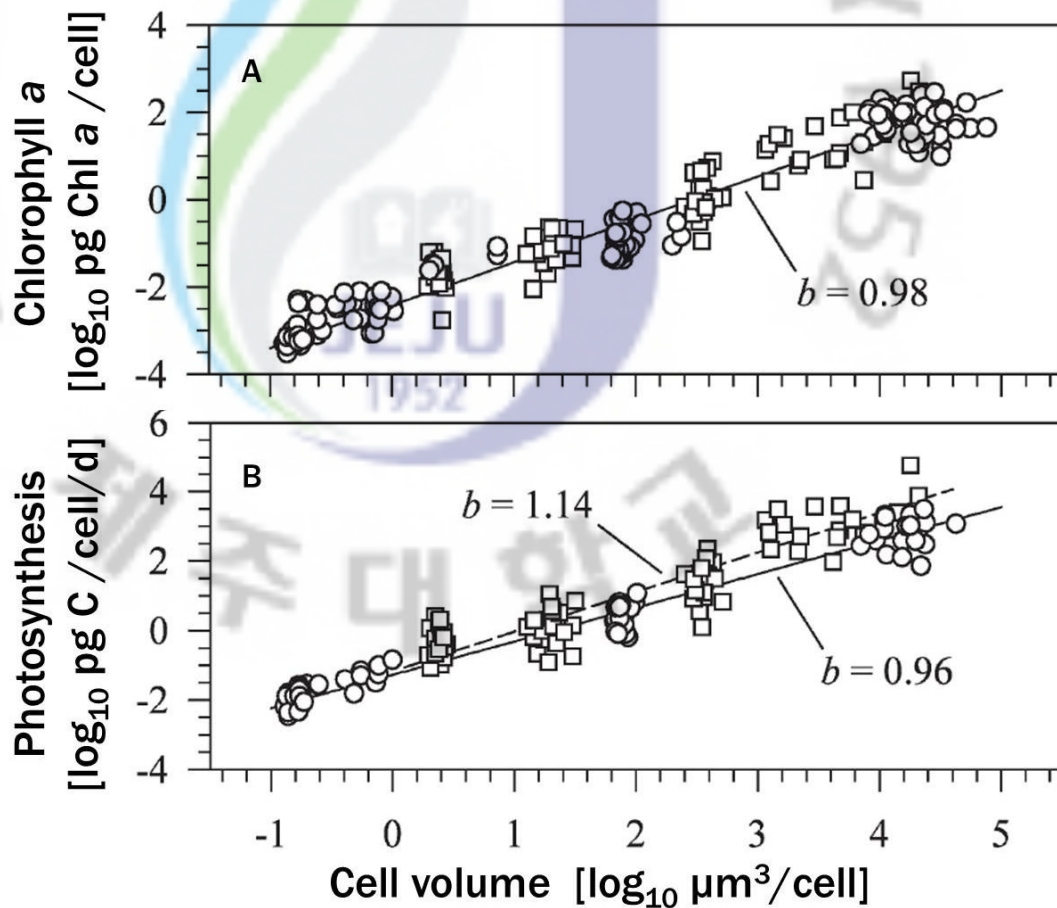
Figure 3.6. Chlorophyll *a*-cell size relation (A) and photosynthesis–cell size relation in phytoplankton (B). Data from the Atlantic Meridional Transect (50ºN to 50ºS, circles) and the Ría de Vigo (squares) (Marañón *et al.*, 2007).

3.5 Conclusion

The IBP from *C. polykrikoides* was measured at different numerical abundance values during cultivation using a 5 MHz transducer in the laboratory environment. During cultivation, the numerical abundance of *C. polykrikoides* was increased by dichotomy, resulting in the increase of IBP. However, during the increase of numerical abundance over a total period of cultivation, the daily variation of numerical abundance occurred. This can be explained by the photosynthesis effect on *C. polykrikoides*. As *C. polykrikoides* photosynthesizes, cellular chlorophyll *a* is increased, leading to the increase of cell volume. During the dark period of cultivation, however, the cell volume is decreased because chlorophyll *a* is not produced but is released instead. This is a new approach to understand the relation between the acoustic backscattered power from phytoplankton, especially *C. polykrikoides*, and its photosynthesis. For *in situ* application in the future, the measurement time would be considered due to the photosynthesis effect.

Chapter 4

HIGH-FREQUENCY ACOUSTIC BACKSCATTERING FROM

RED BLOOD CELL

4.1 Introduction

A typical human RBC has a disk diameter of 6–8 μm and a thickness of 2 μm, which is smaller than *C. polykrikoides*. This is why high-frequency ultrasound is needed to measure backscattering from blood for Rayleigh scattering. Their chain-forming tendency (Chien and Jan, 1973; Chien and Sung, 1987; Matsuoka *et al.*, 2008)—RBC aggregation and chain-forming *C. polykrikoides* is similar. They form a chain so that scatterer size can be varied, though the exact shape and mechanism to form a chain are totally different for the two scatterers.

RBCs are the main component in blood, with a hematocrit of around 40% for normal healthy humans. The measurement techniques of RBC aggregation are mostly applicable only under *in vitro* or *ex vivo* conditions (Cloutier *et al.*, 1996; Shehada *et al.*, 1994; van der Heiden, Maurits S. *et al.*, 1995). However, these were accomplished with a power Doppler, a low-frequency, or a Couette flow system which have some limitations. The power Doppler does not provide information regarding the characteristics of blood flow and flow direction. The Couette flow system is not enough to realize a blood vessel flow since one of two boundary moves dragging a fluid. In this chapter, high-frequency UBM was used to get

blood B-mode images from blood *in vitro* with a mock vessel circulation system. To satisfy the Rayleigh scattering, the frequency ranges of 10, 20, and 40 MHz were used for UBM.

4.2 Materials and methods

4.2.1. Blood preparation

In this experiment, fresh porcine blood was used because its aggregation tendency is similar to that of human blood compared with other species of livestock (Yuan and Shung, 1988). Fresh porcine blood was obtained from a local slaughterhouse in a 1 L bottle that was prepared with a solution consisting of 3 g ethylenediamine tetraacetic acid (EDTA) dipotassium salt dissolved in 30 ml saline for anticoagulation. Four different porcine blood samples were collected to confirm the repeatability. Half (500 g) of the fresh porcine blood was used for WB experiments and the other half was prepared for RBC suspension experiments. To prepare the RBC suspension, WB was centrifuged at 2,500 rpm for 15 min to separate the RBCs from the plasma. The plasma and buffy coat layer, including white blood cells, platelets, and other minor cells, were removed. The concentrated RBCs were washed twice with 0.9% normal saline solution buffered to pH 7.4. To prevent crenation of the red cells, 0.5% bovine albumin was added to the saline solution. The concentrated RBCs were stored in a refrigerator at about 4 °C. The desired hematocrit was obtained at a later time by mixing the concentrated RBCs with 0.9% saline solution for the RBC suspension experiments. Blood was circulated in the flow system for at least 1 h before any measurements were made

in order to remove air bubbles inside the loop and to allow the blood to reach room temperature.

4.2.2. Mock flow system and ultrasound biomicroscopy system

A mock flow system was configured by a peristaltic pump (RP-1000, Eyela, Japan), a silicon tube (id4.76/od7.94, Eyela, Japan), a polyethylene terephthalate (PET) tube, a magnetic stirrer (HI 190M, Hanna Instruments, Korea), and two triangle beakers (500 ml, Samduk, Korea) for the steady state flow. The silicon tube was used in the flow system because the minimal tube size for the peristaltic pump was 7.94 mm of outer diameter. However, the tube wall was too thick and the inner diameter was too big to measure the backscattered signals using high-frequency ultrasound, hence, the PET tube was used at the measurement site. The PET tube was fabricated by rolling a 100 μm-thick PET film in to a diameter of 2.5 mm with a length of 15 cm. The measuring site was chosen at one end of the PET tube. Two triangle beakers were used as reservoirs for the blood and to reduce speed fluctuations. The experimental setup is represented in Figure 4.1.

Reynolds number (R_e) is a dimensionless quantity; it is the ratio of inertial forces to viscous forces which helps determine whether a flow is laminar or turbulent. It is defined as

$$R_e = \frac{2r\tilde{V}\rho}{\mu},\qquad(4.1)$$

where $\Box$ is the mean velocity of the flow, r is the radius of the tube, and ρ and μ are the

density and dynamic viscosity of the liquid, respectively, when applied to liquid flow in a circular tube (Reynolds, 1974; Schlichting, 1968). A laminar flow is considered for less than 2,000 of the R_e and a turbulent flow for the higher R_e (Schlichting, 1968). The region between the entrance of the tube and the point where a laminar flow is established is called the inlet. The inlet length, L_{inlet}, is experimentally determined as follows:

$$L_{inlet} = \frac{2k\rho\tilde{V}r^2}{\mu} = krR_e \, , \tag{4.2}$$

where k is a derived constant in the range of 0.057–0.13. In this study, $k = 0.08$ was used for the oscillatory flow (Nichols and O'Rourke, 2005). The parameters for the mock flow system are presented in Table 4.1. The mean velocity was measured by an ultrasound imaging system (Voluson e, GE Healthcare, USA).

Table 4.1. The dynamic parameters of the blood flow

Radius of tube, r [cm]	Density of blood, ρ [g/cm^3]	Viscosity of blood, μ [dyn·s/cm^2]	Derived constant, k
0.125	1.06	0.1 @ 20 ℃	0.08

Measured mean velocity of flow, $\square$ [cm/s]	Reynolds number, R_e	Inlet Length, L_{inlet} [cm]
12	63	0.6
20	106	1.1
28	148	1.5
36	191	1.9
44	233	2.3

High-frequency ultrasound imaging system, the so-called UBM, was configured by a probe (CLI 1600$_{Ti}$, Capistrano Labs Inc., San Clemente, CA, USA) including a 35 MHz broadband acoustic transducer (35$_{Ti}$MHz, Capistrano Labs Inc., San Clemente, CA, USA) with a PC-based ultrasound imaging board (PCB v4.3, Capistrano Labs Inc., San Clemente, CA, USA) as shown in Figure 4.1. Scanning angle was ±10°. The distance from the transducer pivot to the transducer surface was 10 mm, and the distance from the transducer surface to the probe window surface was 1 mm. The other system parameters are tabulated in Table 4.2.
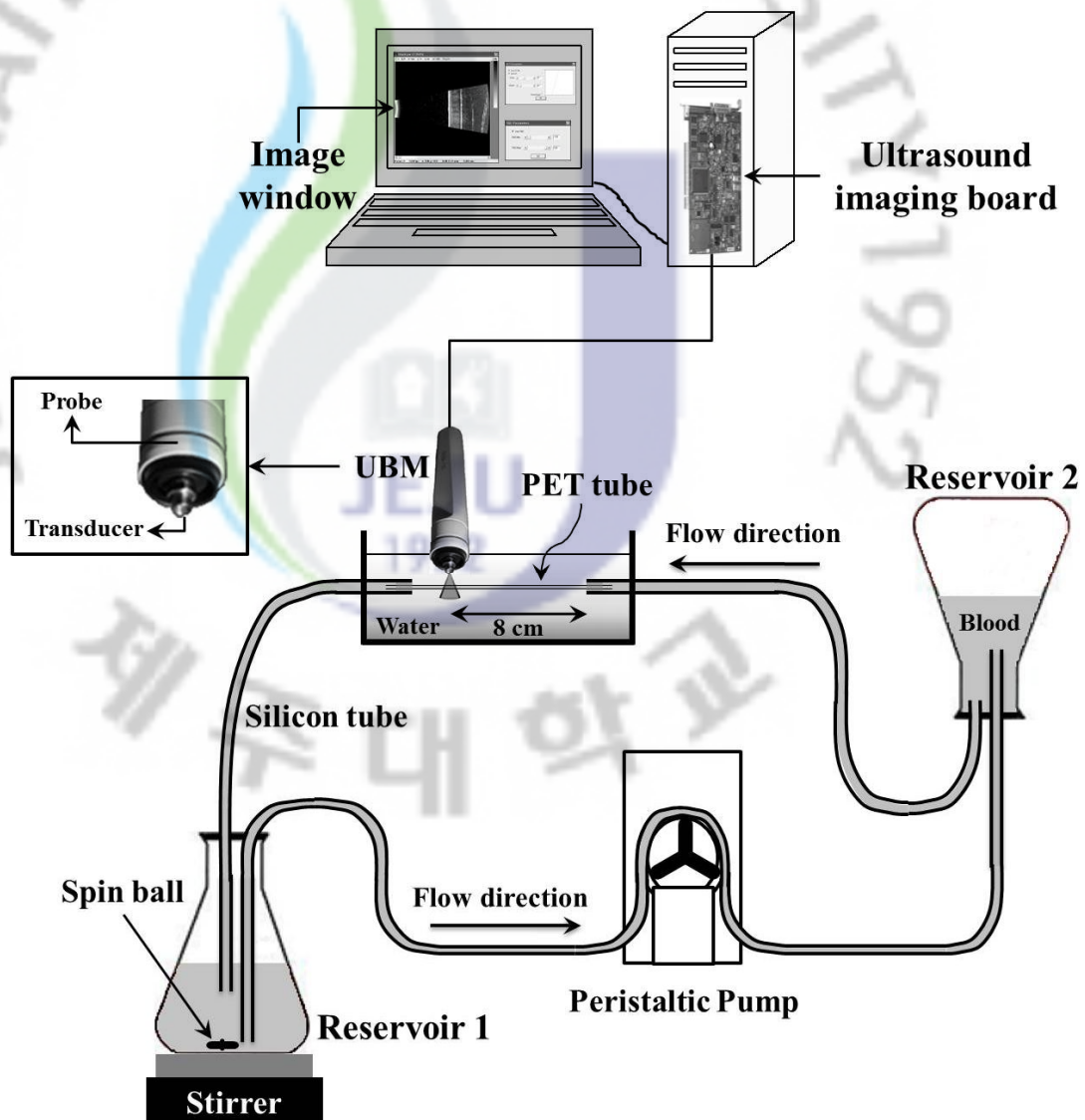
Figure 4.1. Conceptual diagram of the experiment setup for mock flow system and ultrasound biomicroscopy.

Table 4.2. System configuration and parameters of ultrasound biomicroscopy

Configuration	Model	Function	
Probe	CLI 1600$_{Ti}$	Sectorial scan	
Transducer	35$_{Ti}$MHz	35 MHz broad band	
Ultrasound Imaging board	PCB v4.3	Pulser/receiver, image processing	
Parameter		**Value**	
Scanning angle		$\pm10°$	
Transducer pivot to surface		10 mm	
Transducer surface to probe window surface		1 mm	
Frame rate		30 fps	
Frequency		10, 20, 40 MHz	
Amplitude		127.5 (Max.)	
Gain		50	
Jitter control		0	
Scale factor		62	
Offset angle		128 (Center)	
LUT (Look-Up Table)		Center	107
		Window	132
TGC (Time Gain Compensation)		Min.	-21
		Max.	77

4.2.3. Data acquisition and analysis

While the transducer was on sectorial motion with the angle range of ±10º, 256 A-mode scanning lines were acquired in one frame for a B-mode image. The transducer was sectorially reciprocated 30 times per second, and the B-mode image was acquired in one direction so that the frame rate was 30 frames per second (fps). To save data in a PC, 256 frames were saved maximally and data length was 8.5 s approximately.

In the mock flow system, while WB was flowing, B-mode images were acquired at different frequencies (10, 20, and 40 MHz) and mean velocities (12, 20, 28, 36, and 44 cm/s). Therefore, 15 cases of measurement were accomplished. To verify repeatability, three samples of WB were used in the experiment. In the same way, RBC suspension was used after the WB experiment. Three samples of RBCs were used in the experiment for repeatability.

4.3 Results

4.3.1. Blood echogenicity versus blood flow speed for whole blood

Blood echogenicity measured by UBM is dependent on blood flow speed and frequency. In Figure 4.2, as the mean velocity of flow was decreased, the region of interest (ROI) became bright for all frequencies. This result is related to red blood aggregation. RBC forms an aggregate, the so-called rouleaux, in the unstirred suspension. This phenomenon is

47

explained by the physical, physiological, and chemical effects on RBCs. One of physical effects is shear rate. If a fluid media flow with steady state in a vessel, the radial profile of flow speed forms a parabolic shape so that the shear rate becomes different along the radial axis. In addition, as flow speed was increased, the shear rate was also increased and RBCs disaggregate. This means the size of the acoustic scatterer was decreased and the backscattered power from WB was consequently reduced. In this way, blood echogenicity was decreased as flow speed increased, as shown in Figure 4.3. As frequency was increased, the graph of blood echogenicity was downshifted as shown in Figure 4.3-(a) to 4.3-(c). This is thought to be due to either the attenuation at higher frequency or the frequency response of the transducer and the electronic system. Even though blood echogenicity was decreased as frequency was increased, the decreasing patterns of blood echogenicity with flow speed were different at different frequencies. Acoustic scattering from RBC up to around 40 MHz can be explained in the Rayleigh regime.
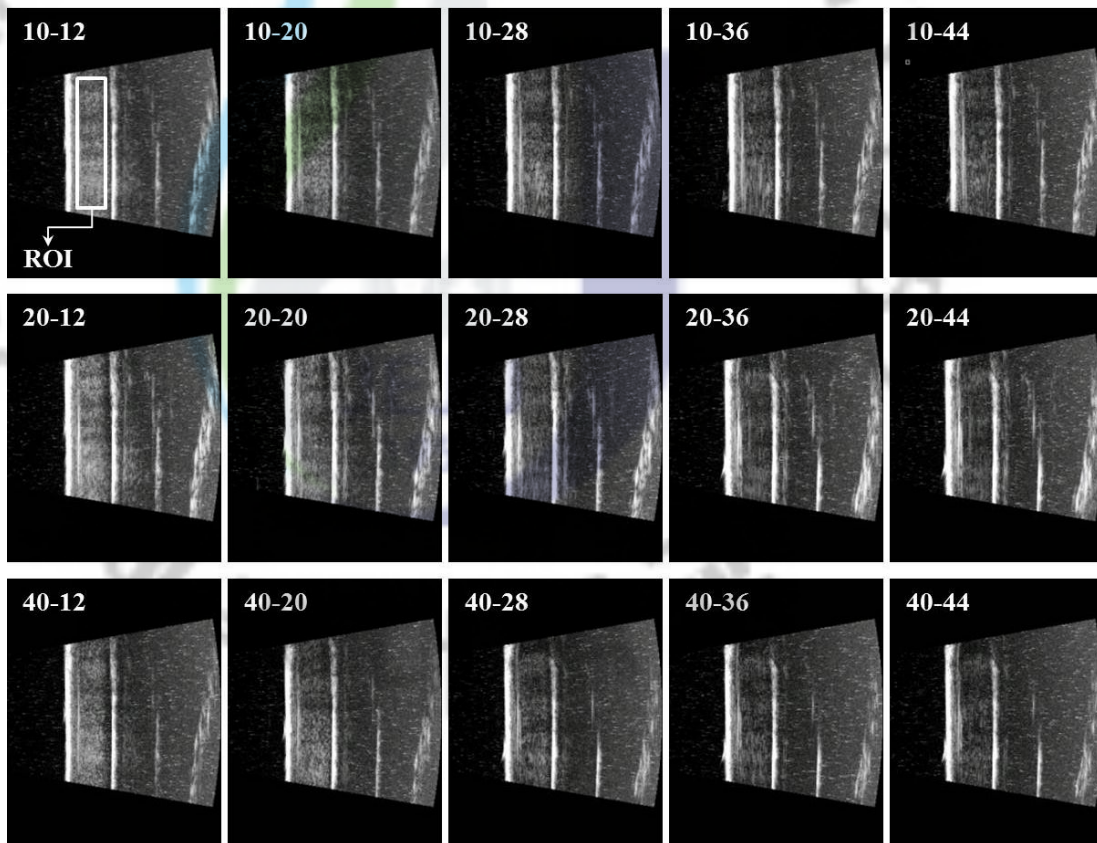
Figure 4.2. Longitudinal ultrasound B-mode image from mock vessel for whole blood. ROI is the region of interest in the image. Each number means frequency–mean velocity for the experimental setup. For example, 10–12 represents 10 MHz–12 cm/s.

Figure 4.3. Echogenicity versus mean velocity of flow depending on frequency (circle: 10 MHz, square: 20 MHz, ×: 40 MHz) for whole blood. The error bar is the standard deviation of the ROI. The mean velocity of flow was varied from 12 to 44 cm/s at each frequency.

4.3.2. Blood echogenicity versus blood flow speed for red blood cell suspension

For the RBC suspension, blood echogenicity was not varied with flow speed (Figures 4.4 and 4.5). This is due to the property of the RBC suspension. Unlike WB, RBC suspension is only RBC suspending media in the saline water, excluding the other components such as fibrinogen, glucose, clotting factors, mineral ions, hormones, and so on. This means the ability to aggregate has disappeared. Thus, there are only Rayleigh scatterers flowing in the media for individual RBCs. Moving speed of the scatterers is not related to the acoustic backscattered power so echogenicity does not vary. As frequency was increased, the graph of blood echogenicity was decreased [Figure 4.4-(a) to 4.4-(c)] like the graph of WB (Figure 4.3).
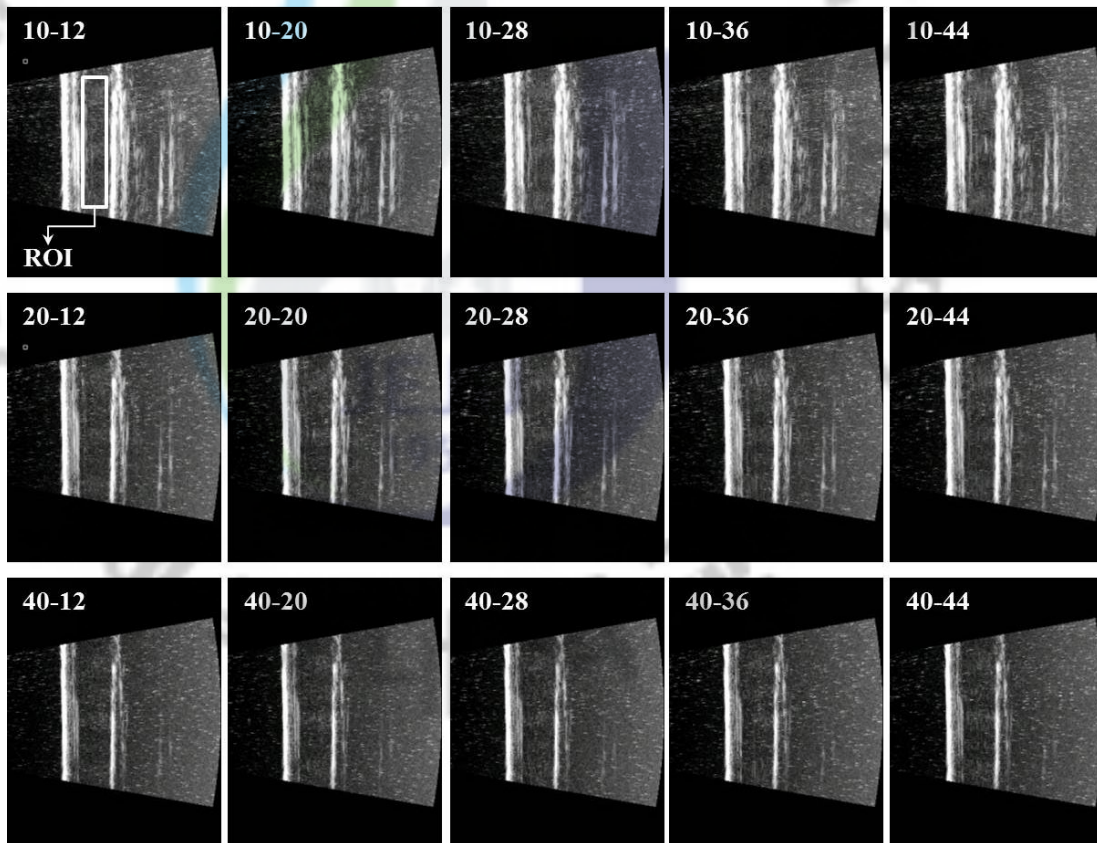
Figure 4.4. Longitudinal ultrasound B-mode image from mock vessel for red blood suspension. ROI is the region of interest in the image. Each number means frequency–mean velocity for the experimental setup. For example, 10–12 represents 10 MHz–12 cm/s.
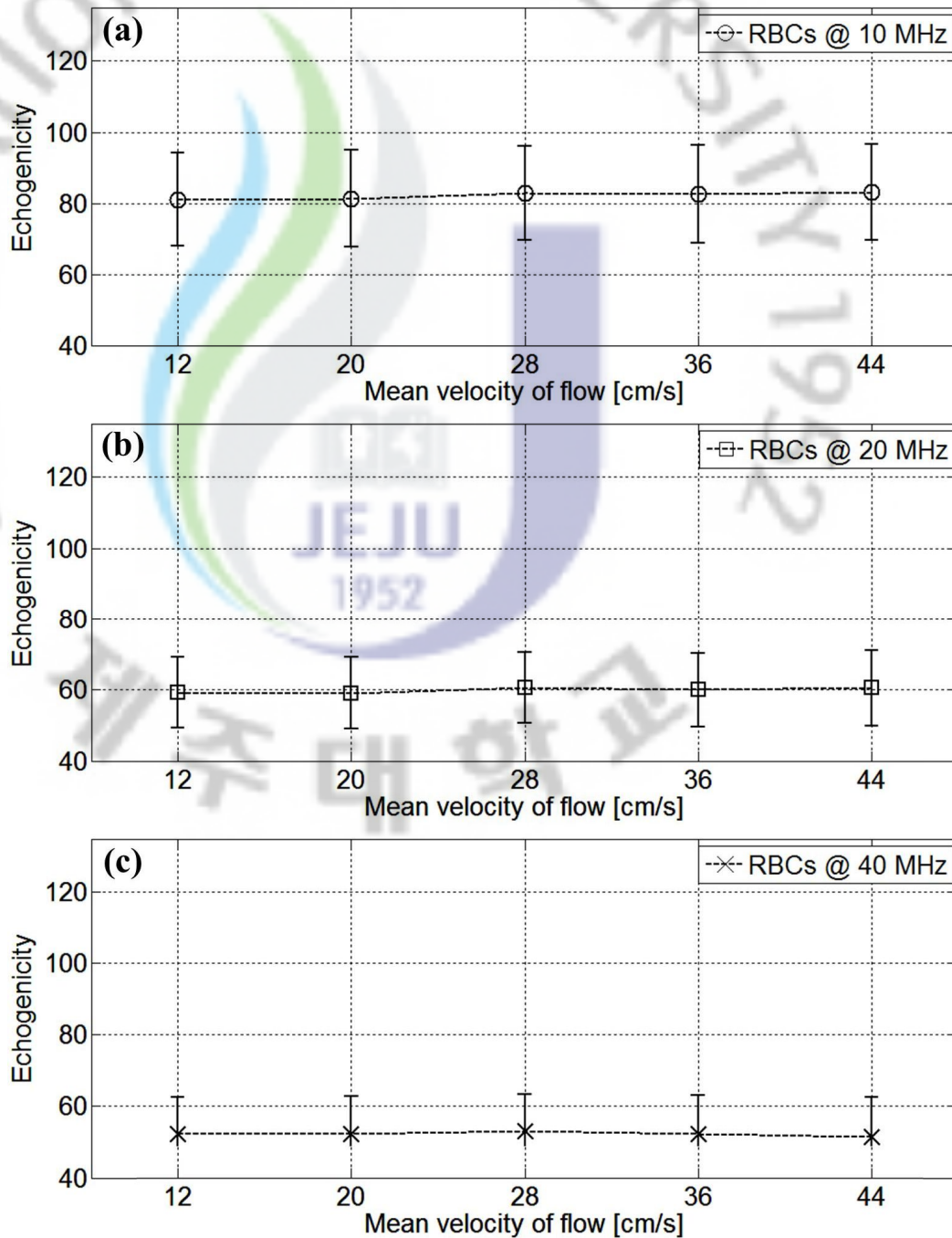
Figure 4.5. Echogenicity versus mean velocity of flow depending on frequency (circle: 10 MHz, square: 20 MHz, ×: 40 MHz) for red blood cell suspension. The error bar is the standard deviation of the ROI. The mean velocity of flow was varied from 12 to 44 cm/s at each frequency.

4.4 Discussion

At low speed, the blood echogenicity from WB was much higher than that from RBCs because the RBCs aggregated at low speed. However, even when RBCs were disaggregated in WB at high speed, the blood echogenicity from WB was still higher than that from RBC (Figure 4.6). RBC suspension includes single RBCs as an acoustic scatterer, whereas WB includes several kinds of scatterers such as RBC, white blood cells, and platelet. However, RBC is a dominant scatterer in WB because of its amount. Therefore, at the same hematocrit and the same measurement set up, the backscattered power from WB is a little higher than that from RBCs at high speed (Figure 4.6). This has been largely reported in previous studies (de Kroon, M. G. M. *et al.*, 1991; Shung *et al.*, 1984; van der Heiden, Maurits S. *et al.*, 1995; Yuan and Shung, 1988) in the frequency range up to 30 MHz with RF signal. In this paper, this phenomenon was also shown at 40 MHz even though it was analyzed by echogenicity, which was processed by unknown nonlinear factors from the UBM system. For WB, as flow speed was increased, echogenicity was decreased due to the disaggregation of RBC at higher shear rate. This corresponds with the findings in previous studies (Shehada *et al.*, 1994; van der Heiden, Maurits S. *et al.*, 1995; Yuan and Shung, 1988).

To verify repeatability of the relation between echogenicity and flow speed depending on the frequency for WB and red blood cell suspension, repetitive measurements were performed with three samples of blood. Decrease of echogenicity depending on flow speed was repeated for the WB and echogenicity was not varied for RBC suspension. For RBC

suspension, the repeatability was quite accurate as seen in the small standard deviation. For

WB, however, standard deviation at low speed was much higher than that at high speed. This
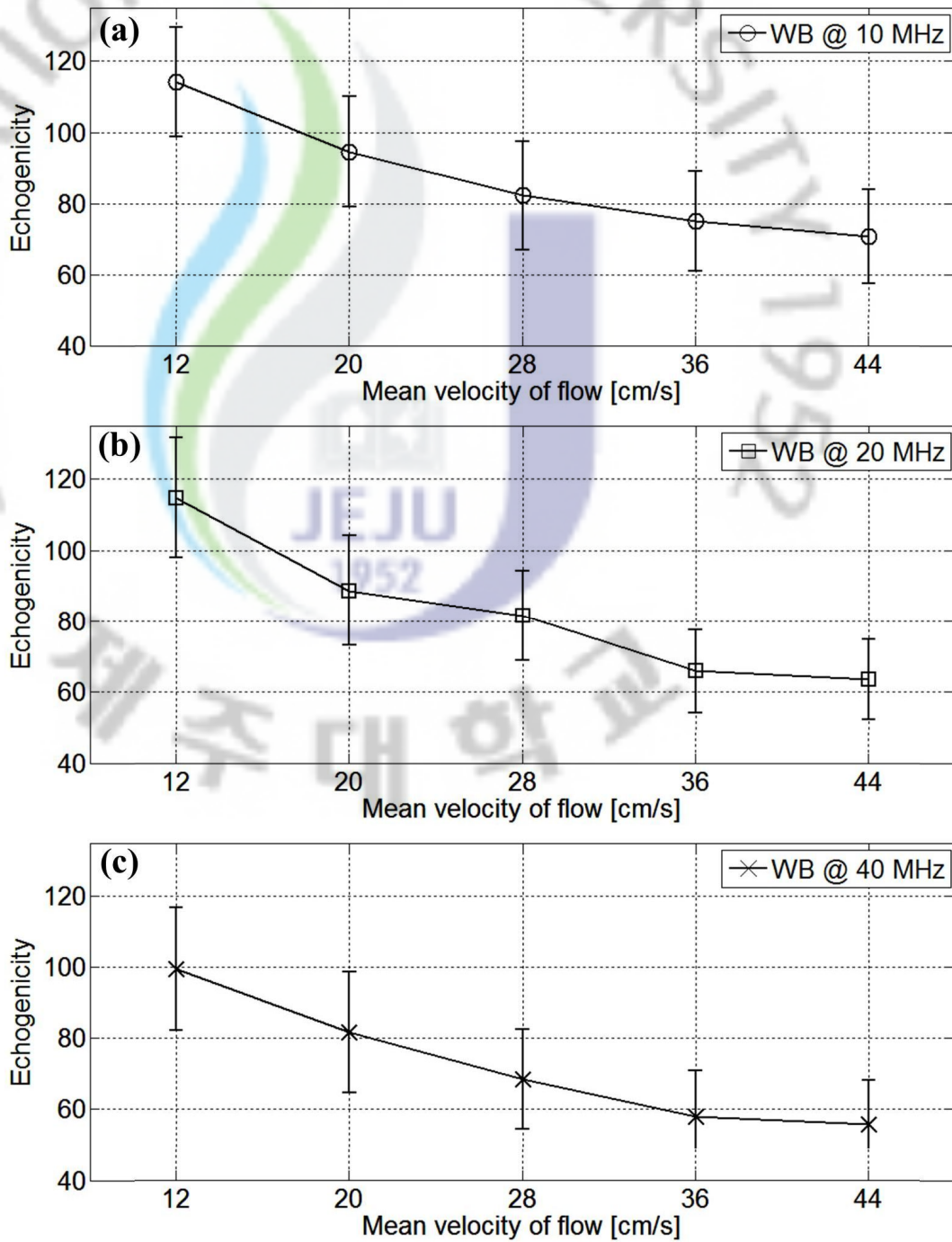
is thought to be the blood property of aggregation.
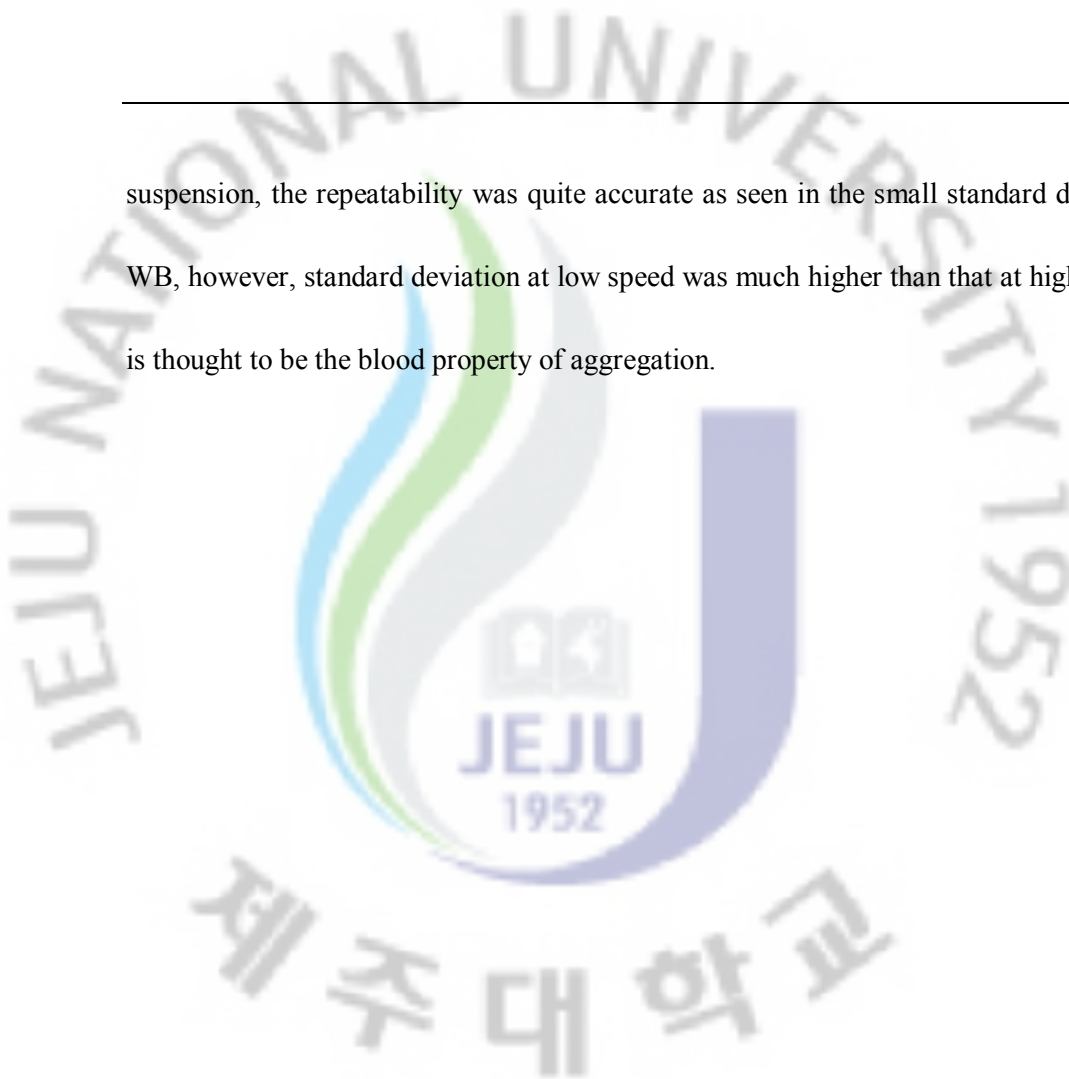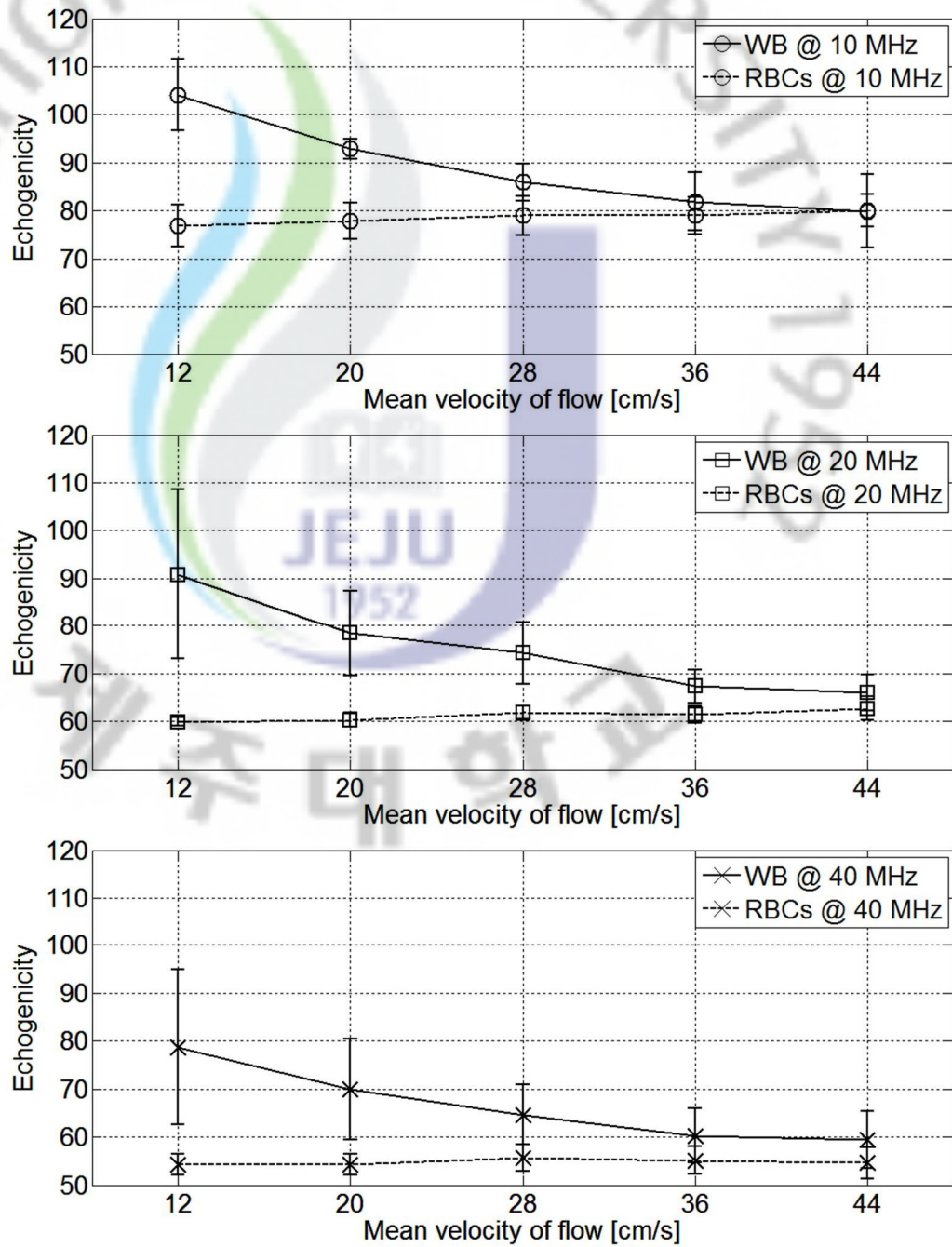
Figure 4.6. Echogenicity versus mean velocity of flow depending on frequency (circle: 10 MHz, square: 20 MHz, ×: 40 MHz) for whole blood (solid line) and red blood cell suspension (dashed line). The error bar is the standard deviation of average echogenicity of three samples. The mean velocity of flow was varied from 12 to 44 cm/s at each frequency.

4.5 Conclusion

The backscattered power from blood is represented by blood echogenicity for an acoustic imaging system such as UBM. In this chapter, blood echogenicity was measured by a UBM in the mock vessel flow system for porcine WB and RBC suspension. Blood echogenicity was increased as flow speed was decreased for WB and was not varied for RBC suspension. This was due to RBC aggregation at low shear rate at low speed, not from a system error of UBM. Based on the results of *in vitro* experiment in this chapter, a high-frequency ultrasound imaging system called UBM can be applied to an *in vivo* experiment in human body. RBCs are known to be Rayleigh scatterers and have an aggregating property in WB. If high-frequency ultrasound up to 30 MHz is applied to human blood vessel, the measurement of RBC aggregation *in vivo* can be conducted.

Chapter 5

BLOOD ECHOGENICITY IN THE RADIAL ARTERY

5.1 Introduction

As mentioned in Chapter 4, RBC is the main component in blood. The clinical effects of RBC aggregation have widely been studied in relation to diseases such as atherosclerosis (Ernst *et al.*, 1991; Koenig and Ernst, 1992; Le Devehat *et al.*, 1990; Schmid-Schobein and Volger, 1976; Volger, 1981) and diabetes (Le Devehat *et al.*, 1990; MacRury *et al.*, 1993; Schmid-Schobein and Volger, 1976; Tanahashi *et al.*, 1993). Therefore, the measurement of RBC aggregation may be useful in diagnosing and monitoring some of these diseases. RBC is the main acoustic scatterer in blood. Hence, blood research using ultrasound have been widely accomplished by measuring the backscattered power or echogenicity, and acoustic methods were studied in order to noninvasively measure the biological tissue (Paeng *et al.*, 2004a; Paeng *et al.*, 2004b; Paeng *et al.*, 2010; Savérya and Cloutier, 2007; Shung *et al.*, 1984; Shung and Cloutier, 1992; Yuan and Shung, 1988; Yuan and Shung, 1988). Recently, *in vivo* measurements of blood echogenicity were performed, but mainly in large arteries (Fatkin *et al.*, 1995; Li *et al.*, 2011; Li *et al.*, 1996; Paeng *et al.*, 2010; Razavian *et al.*, 1995b). These were accomplished at low frequency in a common carotid artery or by intravascular ultrasound. In this chapter, *in vivo* B-mode images were measured in the radial artery using high-frequency UBM. The radial artery at the wrist is positioned approximately 2.5 mm deep beneath the

58

extensor tendons of the thumb, making it relatively easier to measure by ultrasound compared to a carotid artery. High-frequency ultrasound should be used because the radial artery is relatively small. The UBM, which was discussed in the previous chapter, provided high-frequency ultrasound images and was well operated for measuring RBC aggregation in the B-mode image.

5.2 Method

5.2.1. High-frequency acoustic system

The high-frequency acoustic system used in this experiment was the same as the previous one specified in Chapter 4.2.2. The UBM was configured by a probe including a 35 MHz broadband acoustic transducer and a PC-based ultrasound imaging board (Figure 5.1). In addition to this configuration, a nosepiece (PN18923, Capistrano Labs Inc., San Clemente, CA, USA) and a cover film (RB820, Capistrano Labs Inc., San Clemente, CA, USA) were added. To apply UBM to the human wrist in the air, the acoustic impedance should be matched. The nosepiece was fitted into the probe and covered by the thin film after filling with distilled water. The system parameters were the same those presented in Table 4.1, except for the Look-up Table (LUT) and Time Gain Compensation (TGC). LUT displays the grayscale curve used by the system to assign shades of gray to the image and the center (range: 0 to 255) and window (range: 1 to 1024) control the change of the position of the curve and the grayscale assignment. TGC is used to change the relative strength of the

59

displayed echoes from near (range: -128 to +128) and far (range: -128 to +128). LUT and

TGC were optimally set for *in vivo* measurement and presented in Table 5.1.
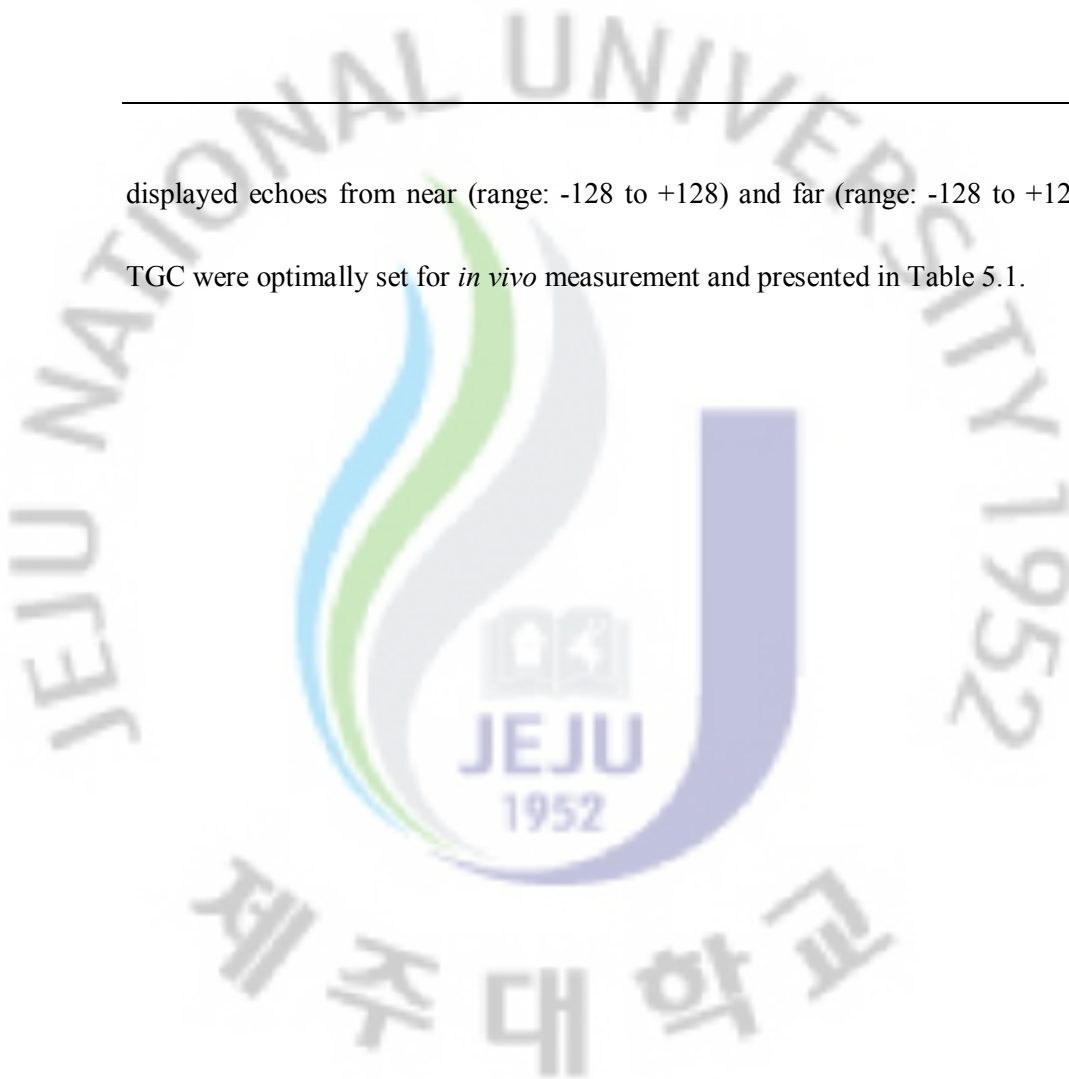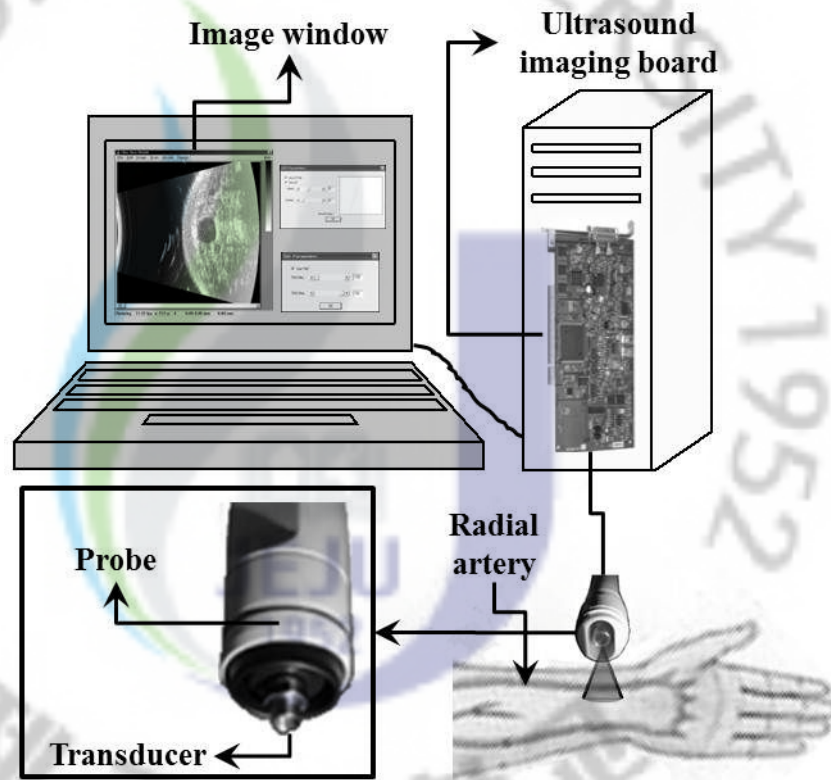
Figure 5.1. System configuration of ultrasound biomicroscopy and conceptual diagram of *in vivo* experiment.

Table 5.1. System parameters of ultrasound biomicroscopy. The others are the same as those shown in Table 4.2.

Parameter	Value	
Frequency	20 MHz	
LUT (Look-Up Table)	Center	36
	Window	108
TGC (Time Gain Compensation)	Min.	-128
	Max.	65

5.2.2. Human subject information and the radial artery

The human subject experiment was approved by the Institutional Review Board (IRB) of the Jeju National University Hospital (grant No. IRB 2009-37). Consent forms were signed by all participants after being briefed on the experimental process, the purpose of the study, and the possible risks involved. Four healthy males aged 31.2 ± 1.3 years old were the volunteers for the *in vivo* experiment. The body mass index (BMI) of the subjects was 25.7 ± 1.7 kg/m^2, and the subjects were a little overweight. To verify the repeatability of the *in vivo* experiment, one of the subjects was chosen for the repetitive measurement. The subject was 31 years old and his BMI was 25 kg/m^2.

The radial artery arises from the bifurcation of the brachial artery in the cubital fossa. It runs distally on the anterior part of the forearm so that it is divided by three branches, the forearm, the wrist, and the hand. Each branch is also divided by several regions (Wikipedia, 2011a). The ROI in this chapter is the radial artery at the wrist (Figure 5.2).
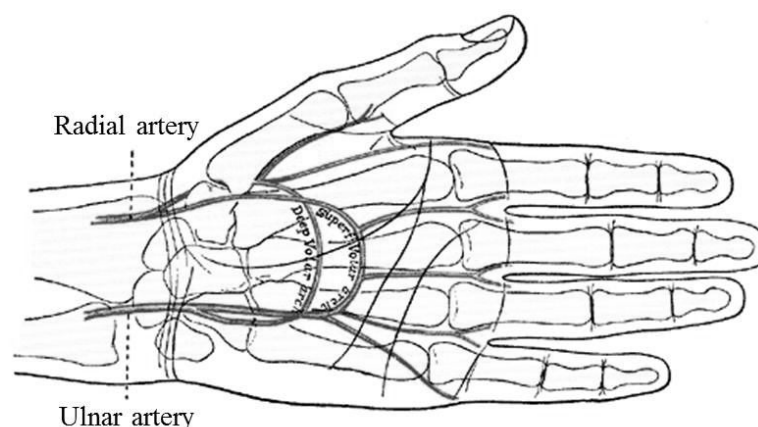
Figure 5.2. Location of radial artery at the wrist (Wikipedia, 2011b).

5.2.3. *In vivo* measurement

The UBM probe was placed on the right wrist near the radial artery after applying a commercial coupling gel to the probe surface. Subjects were then asked to sit on a chair and stay still during examination. Focal zone of the probe was set to the appropriate position of the radial artery by watching the ultrasound image. Gentle pressure was applied to the probe while aligning the focal zone marker to the center of the radial artery. The angle between the probe and the wrist was carefully adjusted to maintain a rounding shape in the cross-sectional images of the vessel (Figure 5.3). While the image was continuously displayed, the last 256 frames were automatically saved as image data after the measurement was stopped. Hence, the measurement was fully kept for 10 s and stopped, and then data were automatically saved in order to obtain 256 frames with 30 fps of the frame rate. To verify the repeatability of the *in vivo* experiment, one subject was chosen for the repetitive measurement. The subject was asked not to take any food and to refrain from smoking on the day of the examination before the measurement. He was also asked not to drink alcohol the night before the measurement. All the measurements were conducted by the same investigator in the morning. The repetitive measurement was performed two times per week for four weeks.

RBC aggregation is much related to the blood flow speed so that flow speed was measured by an ultrasound imaging system (Voluson e, GE Healthcare, USA) for four subjects.

5.2.4. Estimation of region of interest in the radial artery image

Blood echogenicity was calculated as an average over the pixel numbers of ROI in the cross-sectional B-mode images of the radial artery (Figure 5.3). The radial artery is concentrically expanded and contracted due to the heartbeat. The boundary of ROI should be determined because the blood vessel cannot be exactly recognized. Physical property of the radial artery is different from that of other biological tissues around the artery. Therefore, the distribution of blood echogenicity of the radial artery is different from that of other tissues. In this way, if the distribution of blood echogenicity is checked up while varying the area of ROI, then ROI for the radial artery can be optimized.

Kernel density estimation is a nonparametric way to estimate the probability density function (PDF) of a random variable (Epanechnikov, 1969; Rosenblatt, 1956). It is expressed by

$$f(x) = \frac{1}{nh} \sum_{i=1}^{n} K\left(\frac{x - x_i}{h}\right) \ , \tag{5.1}$$

where n is the number of random variables, h is a smoothing parameter called the bandwidth, $K(\cdot)$ is the kernel, and x_i is an independent and identically distributed random variable. Gaussian kernel was used in this chapter. Hence, the Gaussian kernel density estimation was applied to the histogram of blood echogenicity in order to estimate the PDF depending on the area of ROI. The estimated PDFs were also compared to get the optimal ROI from moving radial artery.
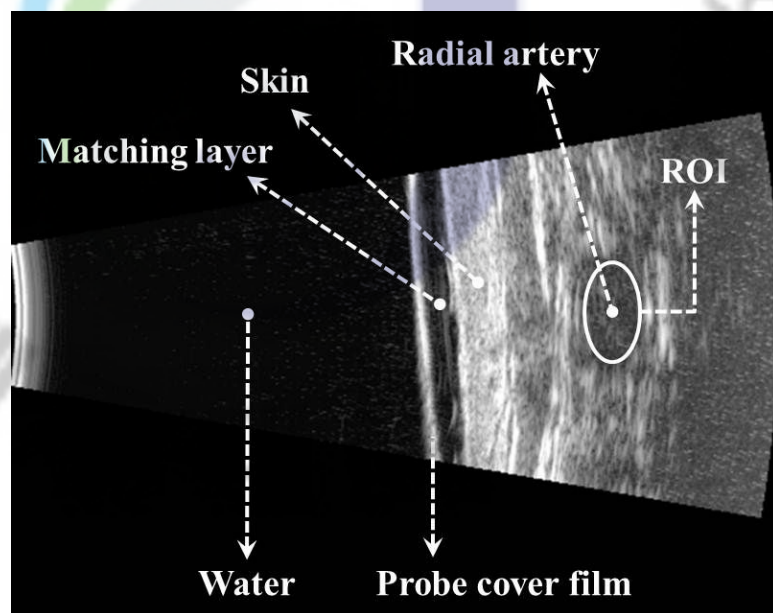
Figure 5.3. Cross-sectional B-mode image of the radial artery. Blood echogenicity was calculated by the pixel number of the ROI.

5.3 Results

5.3.1. Cyclic variation of blood echogenicity

To estimate a boundary between the radial artery and the surrounding tissue, blood echogenicity was measured while varying the area of the ROI. The statistical distributions and estimated PDFs of blood echogenicity were plotted and presented in Figure 5.4. Means and variances at r > 1 (r is relative major axis) were higher than those at r <1. Means of blood echogenicity were 72, 80, 79, 77, and 78 at r = 0.2, 0.4, 0.6, 0.8, and 1, respectively, but were 84 and 95 at r = 1.2 and 1.5, respectively. Variances were 231, 364, 331, 336, and 380 at r = 0.2, 0.4, 0.6, 0.8, and 1, respectively, but were 704 and 1128 at r = 1.2 and 1.5, respectively. This means that if the ROI is larger than r = 1, then the statistical property is changed and echogenicity is measured not only by blood but also by surrounding tissue whose statistical property is different. Means and variances were increased as the ROI was increased. This is because the surrounding tissue affected the increase of the means and variances. The surrounding tissue is a relatively stronger scatterer than blood, so echogenicity from the tissue is higher than that from blood. In this way, the optimal boundary of ROI was determined as r=1 and blood echogenicity was calculated in the ROI of ultrasound image of the radial artery.
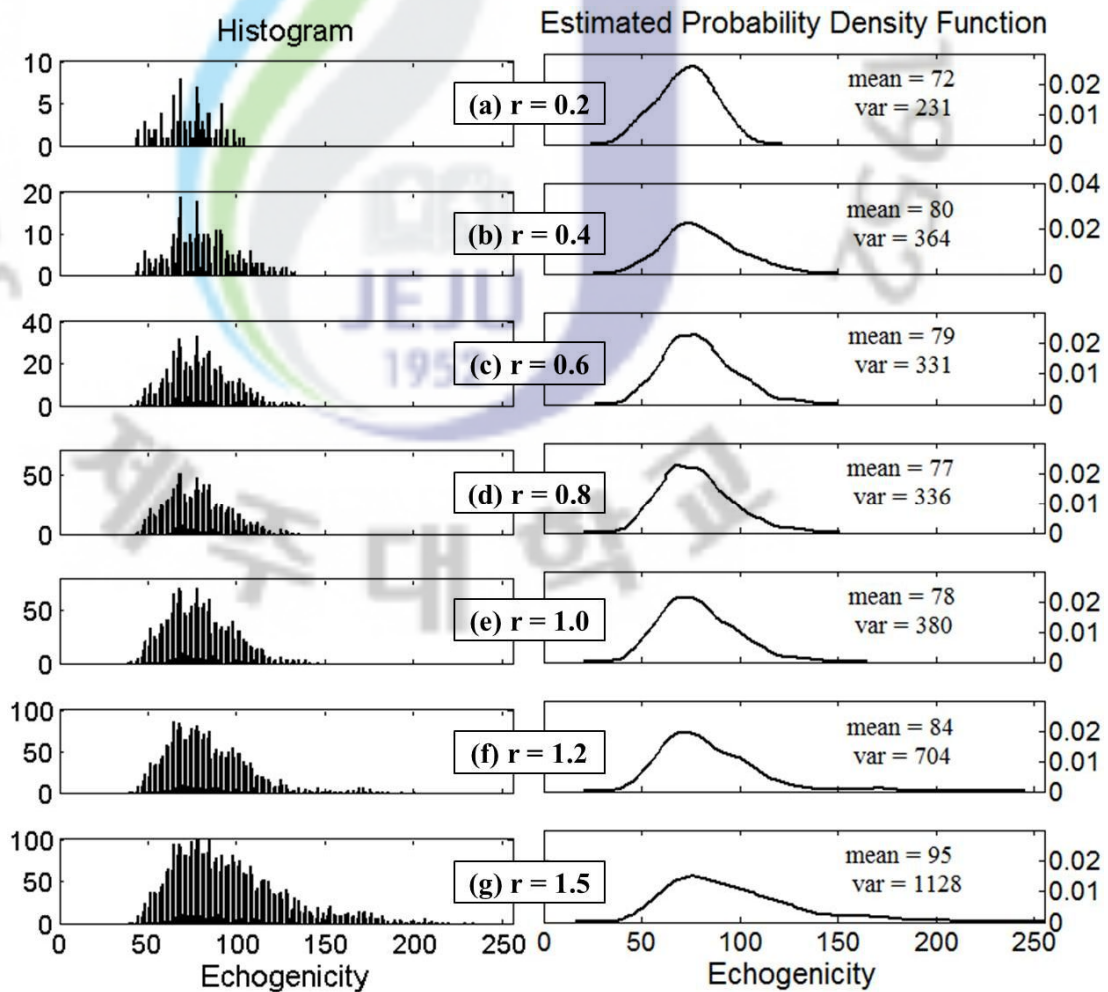
Figure 5.4. Histogram of blood echogenicity (left) and its estimated probability density function (right) depending on the relative major axis (r) of the ROI in Figure 5.3.

In the estimated ROI with r=1, blood echogenicity was calculated for 256 frames which is the limit to save data in a PC. Blood echogenicity was cyclically varied as shown in Figure 5.5. The average and the standard deviation were calculated based on the distribution of blood echogenicity in the ROI. The standard deviation seemed to be cyclically varied, but it was just along the average and not varied greatly. This means that blood echogenicity, which was statically similar, was cyclically varied. The frame rate was 30 fps so that more than 8 s could be approximately calculated. Additionally, the increase and decrease of blood echogenicity were repeated 11 times. In this result, 82 cycles per minute can be estimated, which is similar to the heartbeat rate.
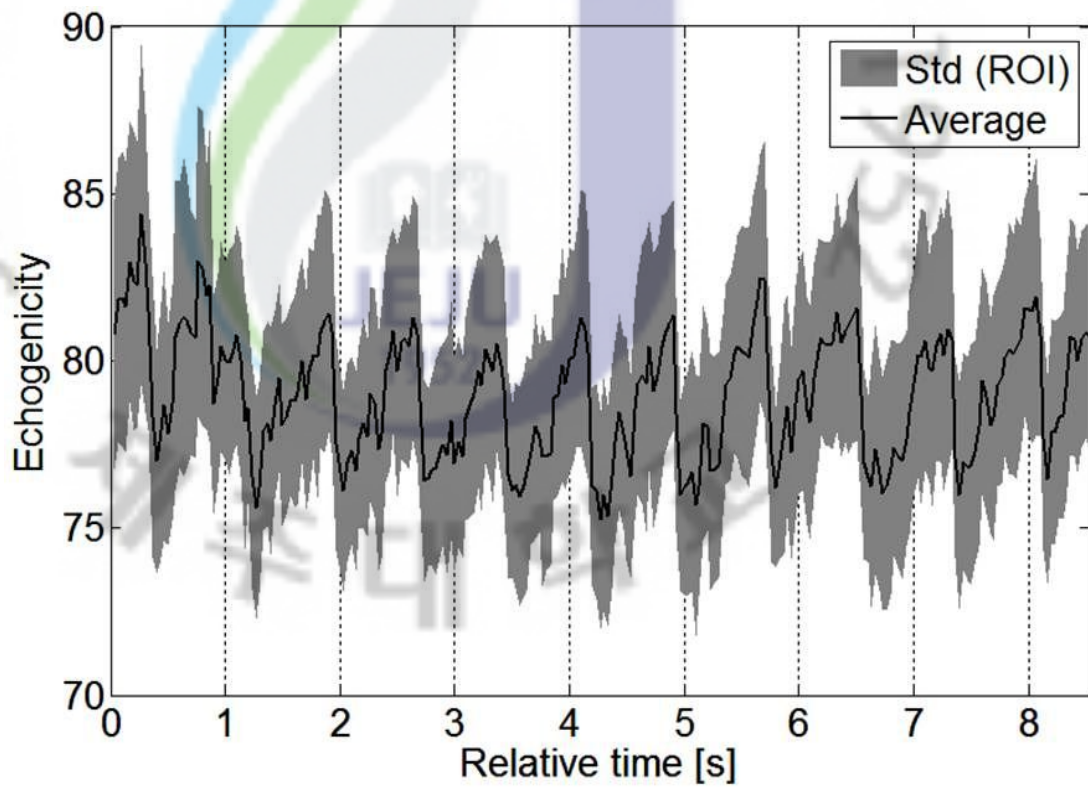
Figure 5.5. Cyclic variation of blood echogenicity in the radial artery. The standard deviation (Std) was calculated by blood echogenicity of ROI. Eleven cycles are seen for 8 s, so that 82 beats per minute can be approximately estimated as a heartbeat rate.

5.3.2. Repeatability of cyclic variation

Cyclic variation of blood echogenicity was observed through an ultrasound B-mode image of the radial artery. Nevertheless, repeatability should be verified for the cyclic variation of blood echogenicity, which would prove to be caused by physiological phenomena not by a system error. In Figure 5.6, cyclic variations were seen for (1) to (6) and (8). This supports the idea that cyclic variation of blood echogenicity is not temporary phenomena in the radial artery. The averaged cyclic variation of blood echogenicity from eight samples is shown in Figure 5.6 (lower panel). The average of the eight samples was also cyclically varied. In the range from 1 to 4 s, the echogenicity was seen as a random variation. This is due to the different data of measurement. Even though one investigator measures the same subject, the cyclic rate can be different. The standard deviation of average result (lower panel of Figure 5.6) was differently defined when compared to each measurement. The standard deviation of the low panel was a standard deviation of eight standard deviation values. This indicates how much standard deviations varied.
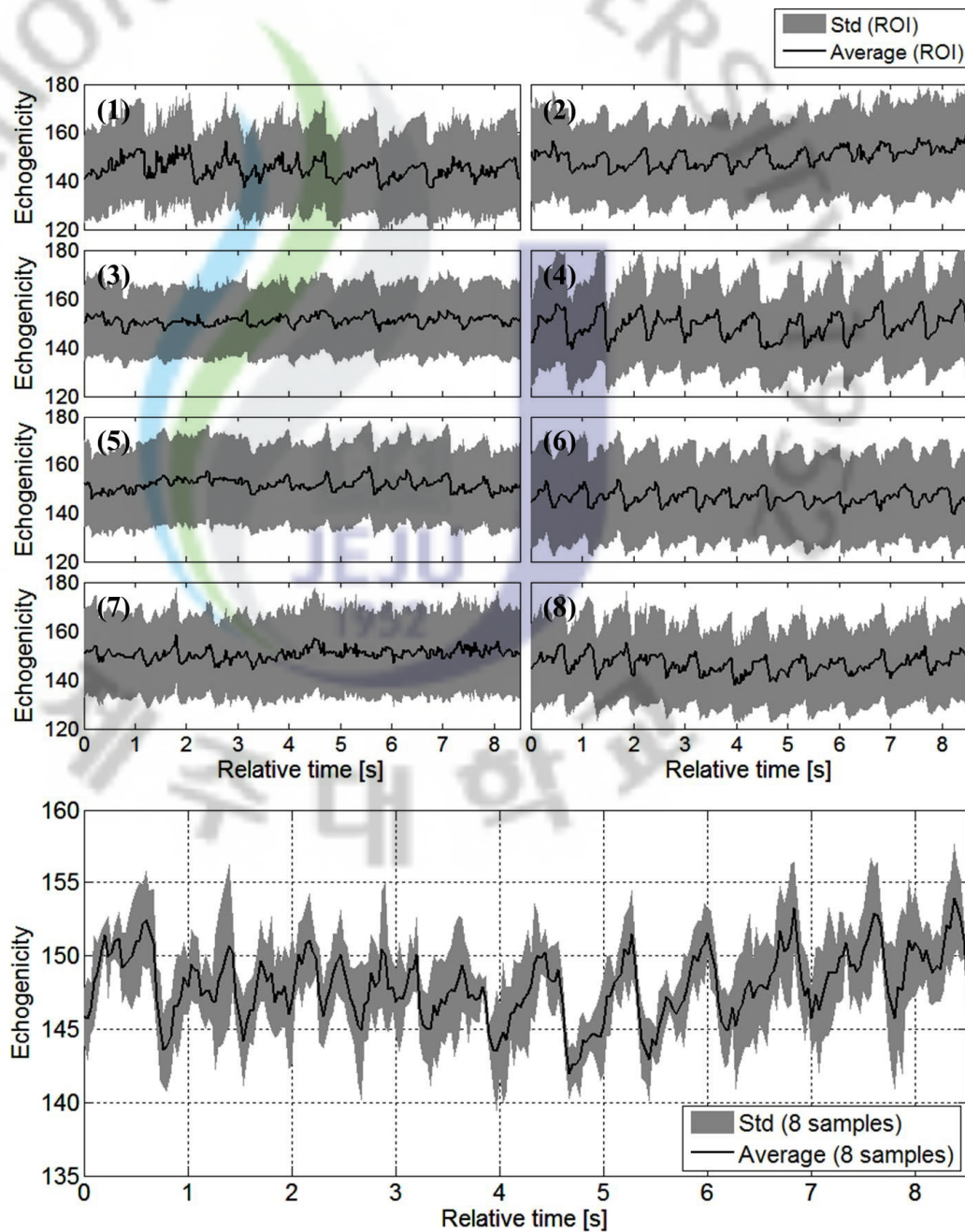
Figure 5.6. Measurement of blood echogenicity for one subject in order to verify the repeatability of cyclic variation of blood echogenicity in the radial artery. The averages and standard deviation (Std) from (1) to (8) were calculated from ROI. In the lower panel, the average was an average of eight averages and Std was a standard deviation of eight standard deviations.

5.4 Discussion

5.4.1. Cyclic variation of blood echogenicity in the B-mode image of the radial artery

Blood echogenicity was measured and studied using the B-mode image, harmonic image, power Doppler, and so on. However, there was no report for the cyclic variation of blood echogenicity to be measured in the radial artery, especially with the B-mode image. The relation between cyclic variation and blood echogenicity was already studied in other papers. Aggregation and disaggregation of RBC result in the cyclic variation of blood echogenicity. In Figure 5.7, the cyclic variation of blood echogenicity was observed in the radial artery using ultrasound B-mode image. Moreover, as mentioned in Chapter 4, blood echogenicity was decreased only for WB as flow speed was increased [Figures 4.6, 4.7, and 5.6(b)]. This explained that cyclic variation was mainly due to the variation of RBC aggregation during a cardiac cycle, because the increase and decrease of blood echogenicity were due to RBC aggregation at lower flow speed and disaggregation at higher speed in the *in vitro* measurement, respectively. The maximal peak is the section of minimal speed (end diastole) and the minimal peak is the section of maximal speed (peak systole). However, RBC aggregation is due to not only flow speed but also shear rate acceleration, and biochemical factors. RBC aggregates as an acoustic scatterer are a stronger scatterer compared to a single cell. When the amount of RBC (hematocrit) is similar under flow, blood echogenicity from RBC aggregates can be cyclically varied.
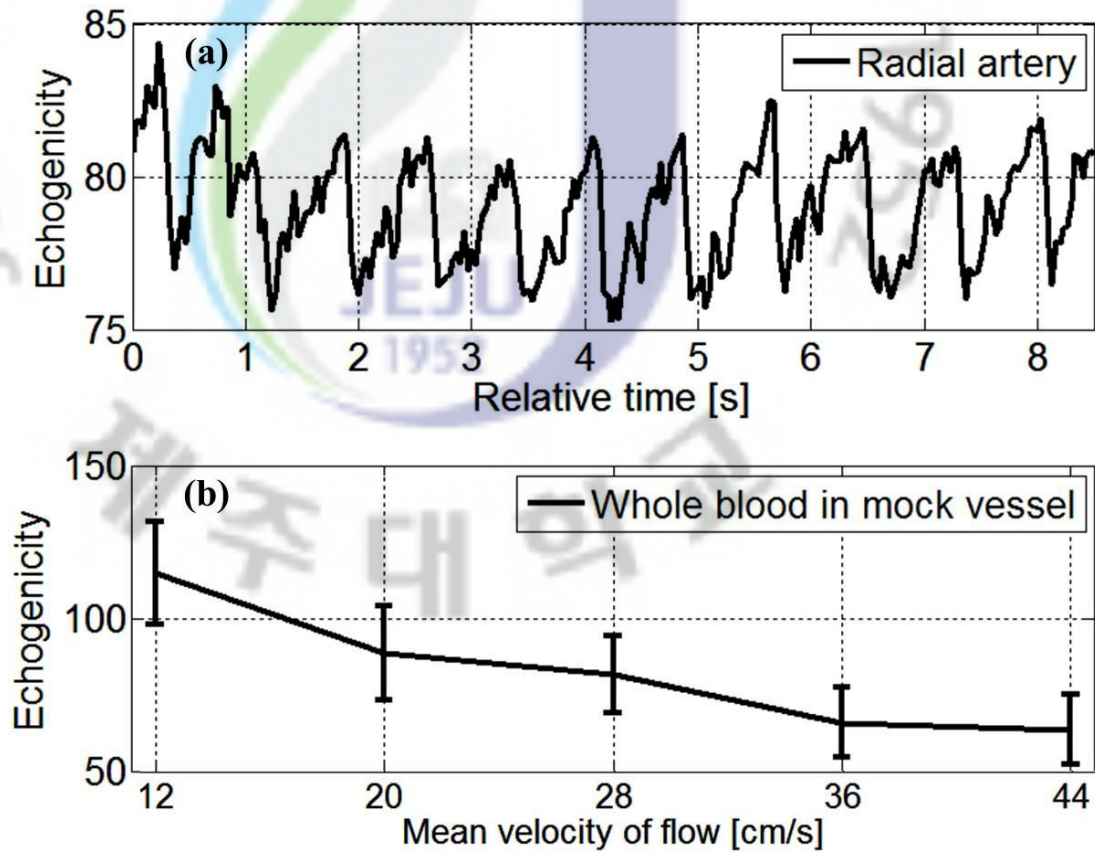
Figure 5.7. Variation of blood echogenicity in the radial artery (a) and in the mock vessel (b).

5.4.2. Statistical analysis depending on section

Particular sections need to be analyzed because blood echogenicity is cyclically varied in the radial artery. In Figure 5.8, eight sections were selected, namely, Max. 1 and 2, Min. 1 and 2, Inc. 1 and 2, and Dec. 1 and 2. At Max. 1 and 2, variances and mean value were higher than the others. When RBCs aggregate maximally, the number of stronger scatterers is increased, that is, the size distribution of the scatterer is also the maximum so that variance of blood echogenicity is high. Oppositely, when RBCs disaggregate maximally, the number of stronger scatterers is decreased, that is, single cells exist so that variance of blood echogenicity is low. On one hand, at both the increasing (Inc. 1 and 2) and decreasing (Dec. 1 and 2) sections of blood echogenicity, mean values and variances were similar to one another, such as 76 for mean values and 305, 302, 301, and 299 for variances. The increasing and decreasing sections are believed to be just a mid-term process between aggregation and disaggregation so that they are not greatly varied.
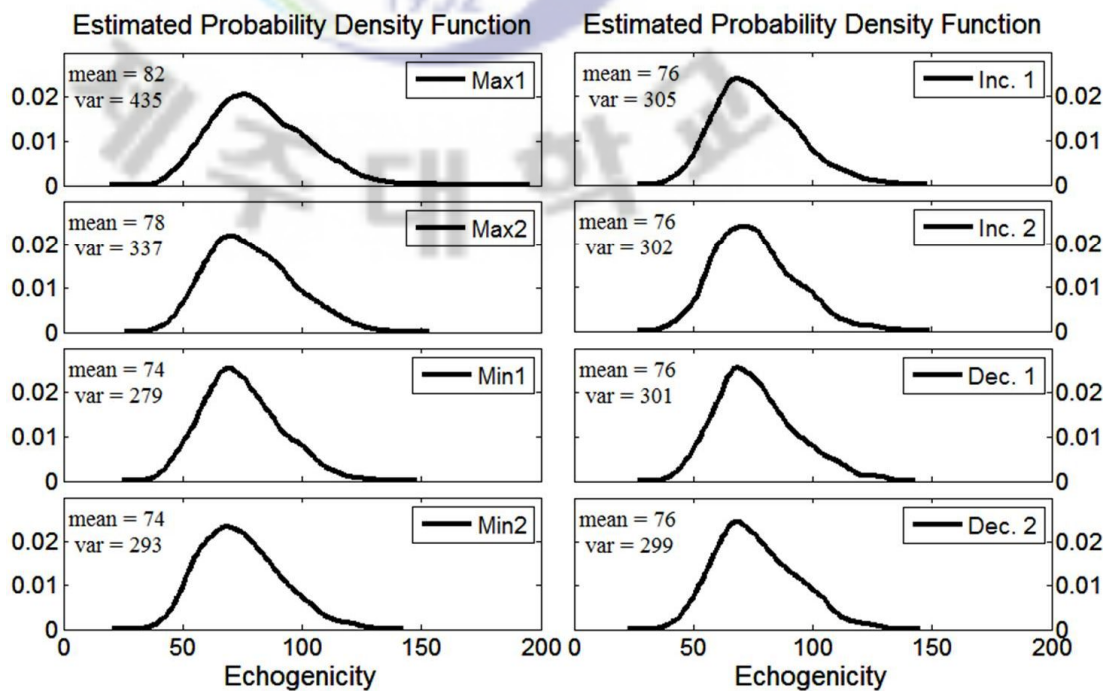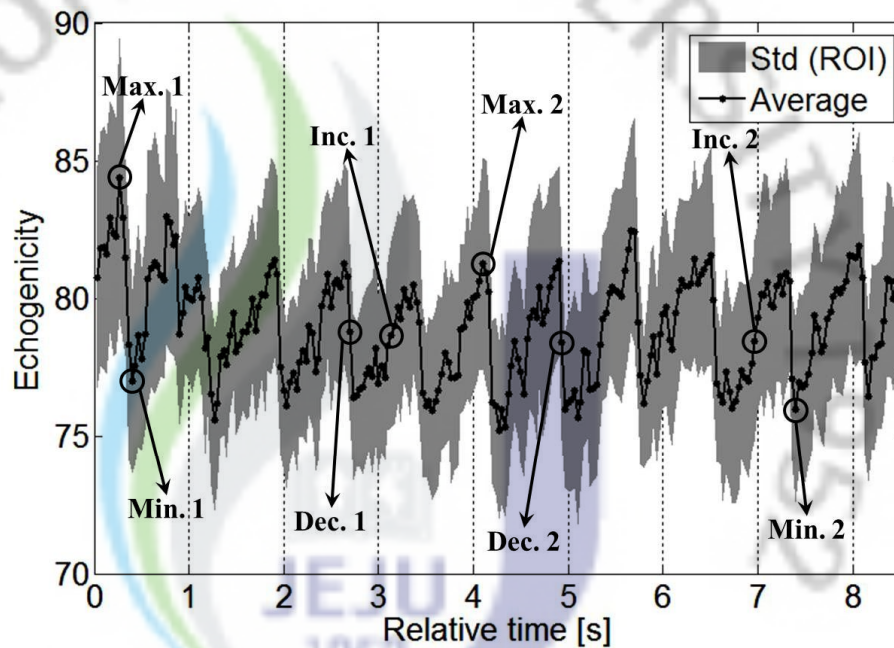
Figure 5.8. Estimated probability density function depending on each particular zone in the cyclic variation of blood echogenicity. The particular zones are divided by the maximal (Max 1 and 2), minimal (Min 1 and 2), increasing (Inc. 1 and 2), and decreasing (Dec. 1 and 2) parts.

In Figure 5.4, PDF was estimated as varying the area of ROI in order to optimize ROI. As the relative major axis (r) decreased, the statistical property was varied. This is related to the inhomogeneous distribution of RBCs in the cross section of the vessel due to the parabolic shape of the velocity profile along the radial axis in the laminar flow. In addition, the number of pixels decreased as r decreased. This means that the number of samples is different in terms of statistical method, so it is not correct to compare the statistical properties. To solve this problem, the statistical property was compared with the same area as shown in Figure 5.9(a–d). The number of pixels in the inner section was the same as that in the outer section. However, the statistical properties of both inner and outer parts were different each other at the maximal peak. The radial variation of blood echogenicity was already studied at peak systole and diastole as shown in Figure 5.9(e) (Paeng *et al.*, 2010). Figure 5.9(a) and (b) show the estimated PDF of the inner and outer parts at maximal peak. The mean values were similar, but the variance of the outer part was higher than that of the inner part. This is explained by the radial profile graph of blood echogenicity at peak systole in Figure 5.9(e). In the range from -0.3 to 0.3, the variation of echogenicity was not much higher than that in the other range. On the other hand, variances of inner part was not much different from that of outer part and mean values also was not at minimal peak. This result was not consistent with the result of diastole even though echogenicity were minimal for two results since arteries are different each other. The vessel diameter and blood flow speed of a CCA are much higher than the radial artery. This would put a different aspect on the result.

76
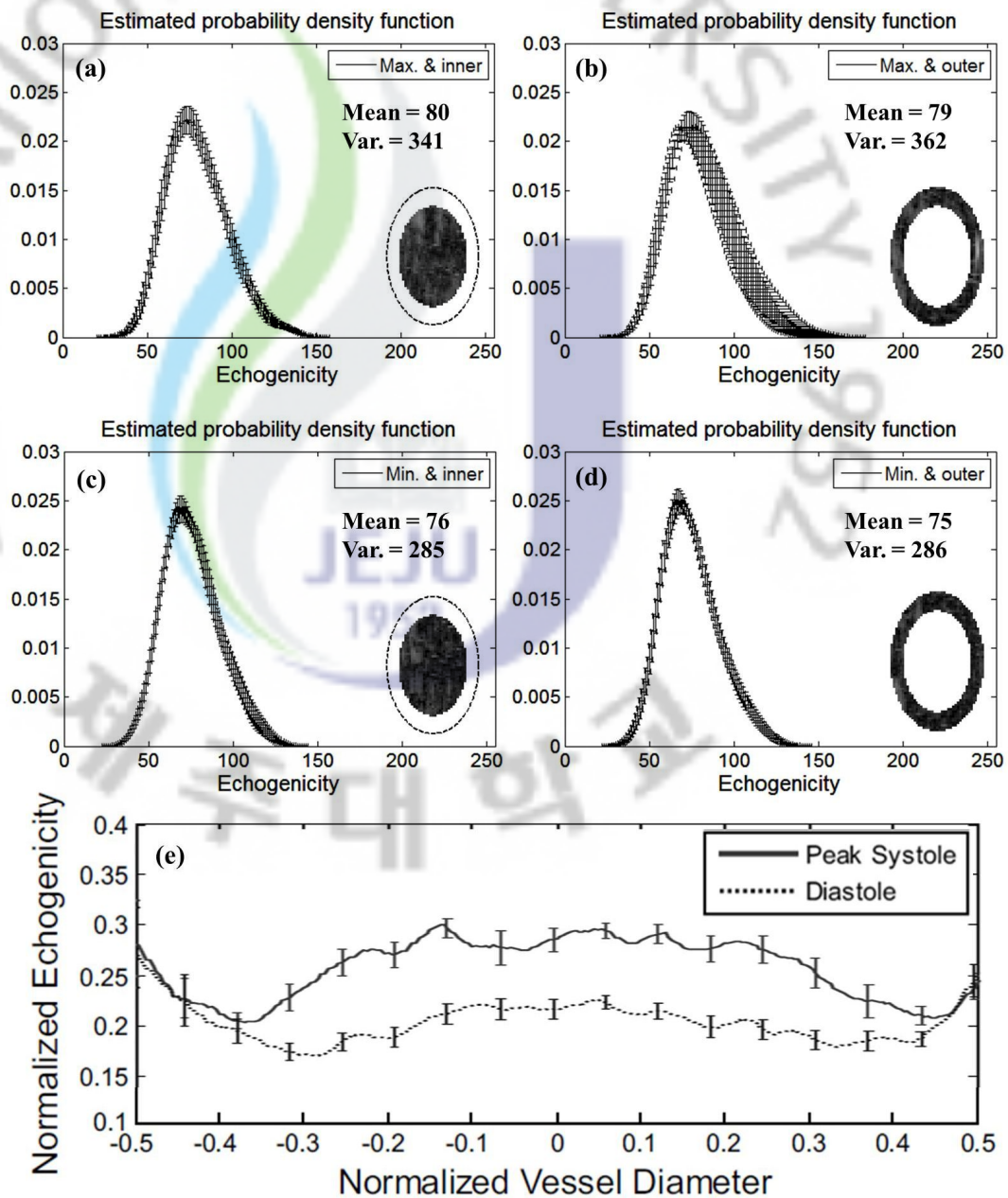
Figure 5.9. Estimated probability density functions of the inner (a) and outer (b) parts for 11 maximal peaks, and the inner (c) and outer (d) parts for 11 minimal peaks. The inner and outer parts are concentric and the same area as shown in each panel. The radial variation of harmonic echogenicity from a carotid artery at peak systole and diastole (e) (Paeng *et al.*, 2010). Data were computed from six volunteers (averaged over nine cardiac cycles per individual) and are represented as the mean 6 standard error.

5.4.3. Radial artery versus common carotid artery in terms of the relation between blood flow speed and blood echogenicity

In the B-mode image of the radial artery (Figure 5.3), the vessel diameter (the distance between proximal and distal axes) and the blood echogenicity can be estimated. The relative diameter and blood echogenicity were plotted and presented in Figure 5.10-(a). As the vessel diameter was increased, blood echogenicity was decreased. The vessel diameter was increased at systole and the blood flow speed was maximal so that the blood flow speed and blood echogenicity were out of phase in the radial artery as shown in Figure 5.10-(a). In the common carotid artery, however, the blood flow speed and blood echogenicity were in phase as shown in Figure 5.10-(b) (Paeng *et al.*, 2010). This can be explained by the blood flow speed. The maximal flow speeds were 17.85 cm/s [Figure 5.10-(c)] and 55 cm/s in the radial artery and the common carotid artery, respectively. The vessel diameters of the radial artery and the common carotid artery are 2.5 and 8 mm, respectively. The two arteries are quite different physically and hemodynamically. The relation between blood flow and RBC aggregation was studied as shown in Figure 5.10-(d) (Paeng and Shung, 2003). At 20 bpm of stroke rate, velocity and Doppler power were almost out of phase, but they were in phase at 60 bpm. The maximal flow speed was decreased as stroke rate was decreased. This lower stroke rate can be considered as the radial artery so that the velocity and blood echogenicity variation were out of phase. Blood echogenicity was mainly governed by the shear rate when the acceleration was small. However, the acceleration became more important when

78

compared to the shear rate because both stroke rate and maximal flow speed were increased.

The combined effects of shear rate and acceleration might change the variation pattern. This

higher stroke rate can be considered as the common carotid artery so that the variations were

in phase.
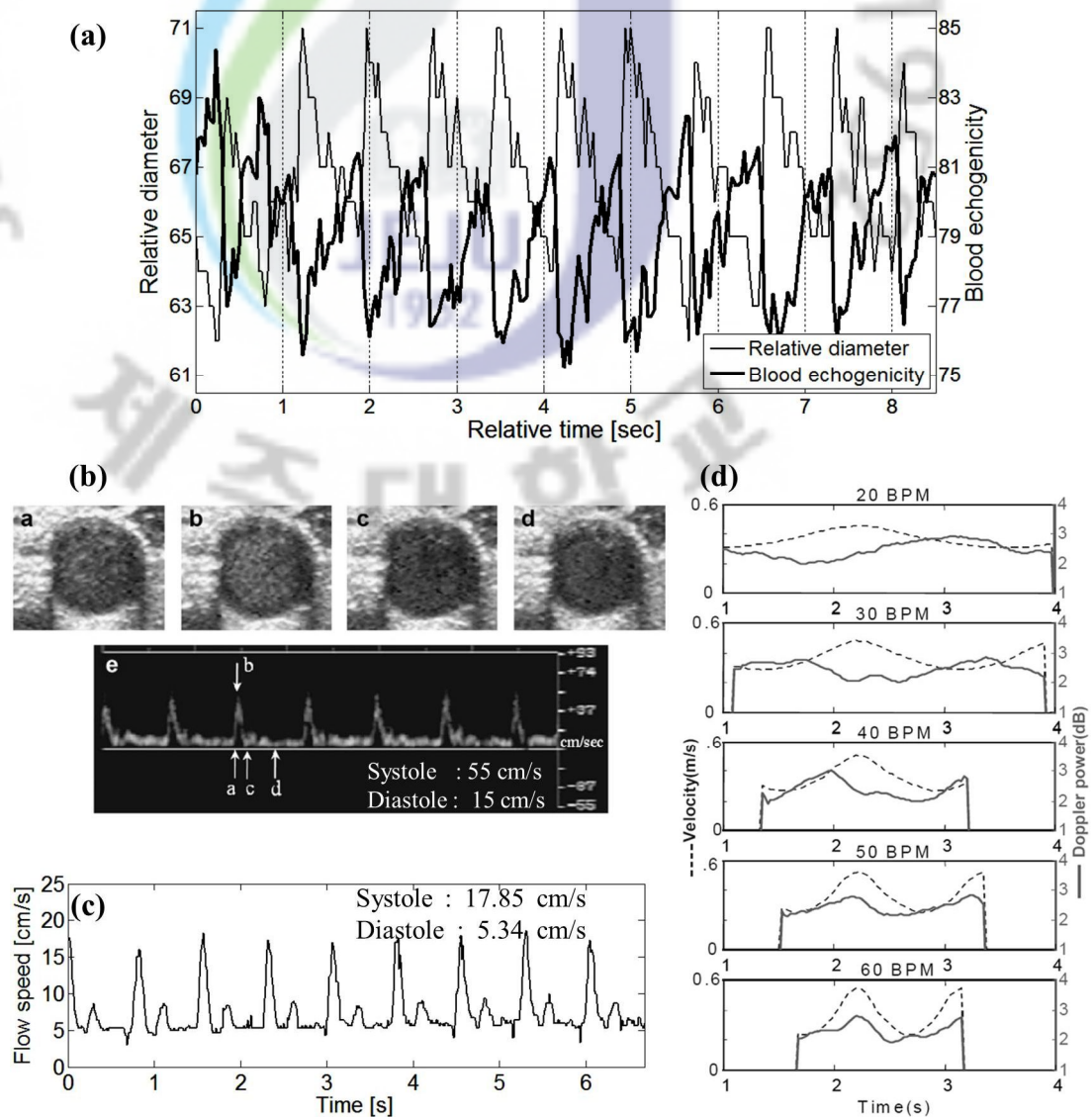
Figure 5.10. Relation between blood echogenicity and blood flow speed at the radial artery
(RA) and the common carotid artery (CCA). (a) The relative diameter of vessel and the

blood echogenicity were out of phase in the RA. (b) The blood flow speed and the blood echogenicity were in phase in the CCA (Paeng *et al.*, 2010). (c) 5–18 cm/s of blood flow speed at the RA. The vessel diameter is maximal at systole. (d) The blood flow speed and the blood echogenicity became in phase as the flow speed was increased (Paeng and Shung, 2003).

It is very complicated to theoretically analyze pulsatile flow such as the radial artery and the common carotid artery. For the simple approach, these arteries can be considered as an oscillatory flow assuming a Newtonian fluid, a laminar flow, a long vessel with constant diameter, and a single sinusoidal flow. The oscillatory flow was analyzed by Womersley in a rigid cylindrical tube (Womersley, 1955). The Womersley number (α) is a dimensionless number to keep dynamic similarity and is defined as

$$\alpha = r\sqrt{\frac{\omega\rho}{\mu}} \tag{5.2}$$

where r is the radius of the tube, ω is the angular frequency of the oscillation, and ρ and μ are the density and dynamic viscosity of the liquid, respectively. The parameters and the Womersley numbers for the radial artery and the common carotid artery were tabulated (Table 5.2). When α is small (1 or less), the frequency of pulsations is sufficiently low so that a parabolic profile of velocity has time to develop during each cycle. The flow will also be very nearly in phase with the pressure gradient, which will be given to a good approximation by Poiseuille's law, using the instantaneous pressure gradient. On the other hand, when α is large (10 or more), the velocity profile is relatively flat, and the mean flow

lags the pressure gradient by about 90º. The Womersley number determines the dynamic similarity along with the R_e. Since the RA (small α) is hemodynamically different from the CCA (large α), RBC aggregation in the RA was different from that in the CCA during a cardiac cycle. Echogenicity was maximal at end diastole and minimal at peak systole in the RA. On the other hand, echogenicity was maximal at peak systole and minimal at end diastole in the CCA. The phase of cyclic variation between the RA and the CCA was opposite each other. According to *in vitro* experiments in Chapter 4, blood echogenicity was increased as blood flow speed was decreased. This result was consistent with cyclic variation of blood echogenicity in the RA since the blood flow speed was low and the Womersley number, α was small in the RA. In contrast with the RA, blood echogenicity was decreased as blood flow speed was decreased in the CCA. This is because blood flow speed was high and Womersley number, α was large in the CCA.

Table 5.2. The dynamic parameters for the Womersley number of the radial artery and the common carotid artery

		Radial artery	Common carotid artery
Radius of vessel, r [cm]		0.12	0.4
Flow speed [cm/s]	Peak systole	17.14 ± 0.96	55 (Figure 5.10-(b))
	End diastole	3.37 ± 1.39	15 (Figure 5.10-(b))
Angular frequency of oscillation, ω		7	
Density of blood, ρ [g/cm^3]		1.06	
Dynamic viscosity of blood, μ [dyn·s/cm^2]		3.5×10^{-3} @ 37 ºC	
Womersley number, α		1.4	5.8

82

5.5 Conclusion

Blood echogenicity was measured using high-frequency ultrasound and its cyclic variation was observed in the radial artery. The cyclic variation of blood was inferred from RBC aggregation. Blood echogenicity was decreased as blood flow speed was increased under steady flow. Based on this result, as blood flow speed was cyclically varied under a cardiac cycle, the variation of blood echogenicity was clarified. This is thought to be the first observation of the cyclic variation of the the B-mode echogenicity in the radial artery. In the previous study, cyclic variations of blood echogenicity have been measured, but these were measured in the harmonic image of a common carotid artery. In terms of measurement type and target, this chapter describes a new approach to measure blood echogenicity. The radial artery is positioned in the wrist so that it is relatively easier to measure by ultrasound. In particular, the radial artery is well known as a pulse wave diagnosis in oriental medicine. The pulse is due to the expansion and contraction of the elastic walls of the radial artery through the action of the heart upon the column of blood in the arterial system. Therefore, if the results of this chapter are studied with the pulse wave in the radial artery, then more information about the radial artery would be accomplished.

Chapter 6

CONCLUSIONS AND SUGGESTIONS

6.1 Conclusions

In this research, high-frequency acoustic backscattering from both *C. polykrikoides* in the cultivating medium and RBC in blood was measured in the Rayleigh regime. Both objects are weak scatterers, so a high-frequency ultrasound was used in the measurement of backscattering. The backscattering variations were observed during measurement of the two scatterers.

The IBP from *C. polykrikoides* was increased because *C. polykrikoides* reproduced asexually by binary fission and formed chains while the cultivation proceeded. This was well explained by the relation between the IBP and the number of scatterers. The backscattered power is proportional to the volume backscattering strength and the number of scatterers. Therefore, the acoustic backscattered power was increased as the number of scatterers, *C. polykrikoides*, was increased. During cultivation, however, the IBP from *C. polykrikoides* was varied daily when the light was turned on and off. This is different from the relation between the IBP and the number of scatterers. As the cell volume is increased while phytoplankton photosynthesizes, the IBP can be increased during light because the volume of *C. polykrikoides* is increased due to photosynthesis. However, the IBP is decreased during darkness because the volume of *C. polykrikoides* is decreased. The photosynthesis effect is

an explanation because the change of *C. polykrikoides* volume was not measured. Nevertheless, the IBP variation depending on the illumination might be the reasonable result because the photosynthesis effect on the phytoplankton was well represented.

The blood echogenicity from porcine WB was decreased at higher flow speed and increased at low flow speed. However, the blood echogenicity from RBC suspension was not varied even though the flow speed was changed. These phenomena were explained by RBC aggregation in WB. At low speed, the shear rate was relatively low so that RBCs aggregated and then the blood echogenicity was increased. Based on these results, the cyclic variation of blood echogenicity in the RA can be explained. The blood echogenicity was increased because of RBC aggregation at low speed under pulsatile flow during a heartbeat cycle. The cyclic variation of blood echogenicity was observed by high-frequency ultrasound in the RA. The variation of blood echogenicity in the RA was similar with that in *in vitro* experiment due to low flow speed and small Womersley number. But this result was opposite with the CCA because of different dynamic characteristics. This means the relation between RBC aggregation and blood flow depends on the blood vessel. We confirmed that RBC aggregation was measured by acoustical method and hemodynamical phenomena can be analyzed by ultrasound. This would be helpful for the development of noninvasive blood research using acoustics.

6.2 Suggestions for future studies

As mentioned in the experiment for *C. polykrikoides*, the change of *C. polykrikoides* volume should be measured for further analysis. To do this, chlorophyll *a* should be measured during cultivation. Photosynthesis was already reported to be proportional to chlorophyll *a* for phytoplankton (Marañón *et al.*, 2007), which explains how the IBP from *C. polykrikoides* is increased during photosynthesis. As well as *C. polykrikoides*, other phytoplankton can be similarly studied by acoustic methods.

The viscosity of blood depends on RBC aggregation, and RBC aggregation depends on shear rate and other factors such as viscosity, acceleration, and so on. Hence, a more accurate analysis would be possible for the variation of blood echogenicity in the radial artery. Moreover, the clinical application is needed for diagnosis such as a comparative study between experimental and control groups. The vessel motion and the blood flow make the unique pulse wave in the RA. And the unique pulse wave has been utilized for the diagnosis of various diseases by the oriental medical doctors. Hence the quantitative analysis of the pulse wave should be studied.

BIBLIOGRAPHY

Ahn Y-, Shanmugam P, Chang K-, Moon J- and Ryu J-. Spatial and Temporal Aspects of Phytoplankton Blooms in Complex Ecosystems Off the Korean Coast from Satellite Ocean Color Observations. Ocean Science Journal 2005;40:67-78.

Anderson VC. Sound Scattering from a Fluid Sphere. J. Acoust. Soc. Am. 1950;22:426-431.

Armstrong JK, Meiselman HJ and Fisher TC. Evidence against macromolecular "bridging" as the mechanism of red blood cell aggregation induced by nonionic polymers. Biorheology 1999;36:433-437.

Baumler H, Neu B, Donath E and Kiesewetter H. Basic phenomena of red blood cell rouleaux formation. Biorheology 1999;36:439-442.

Benson K. MCAT Review, Emory University 1999.

Blanc S, Benitez CE, de Milou, M. I. E., Mosto P, Lascalea G and Juarez RE. Acoustic behaviour of phytoplanktonic algae. Acoustics Letters 2000;23:175-182.

Bok T, Paeng D, Kim E, Na J and Kang D. Ultrasound backscattered power from Cochlodinium polykrikoides, the main red tide species in the Southern Sea of Korea. Journal of Plankton Research 2010;32:503-514.

Brooks DE, Russell G, Janzen G, Janzen J. Mechanisms of erythrocyte aggregation. In: Cokelet GR, Meiselman HJ, Brooks DE (Eds.). Erythrocyte Mechanics and Blood Flow. New York: A. R. Liss, 1980. pp. 119-40.

Chien S and Jan K. Ultrastructural basis of the mechanism of rouleaux formation. Microvasc.Res. 1973;5:155-166.

Chien S and Sung LA. Physicochemical basis and clinical implications of red cell aggregation. Clin. Hemorheol. 1987;7:71-91.

Chu D, Stanton TK and Wiebe PH. Frequency dependence of sound backscattering from live individual zooplankton. ICES Journal of Marine Science: Journal du Conseil 1992;49:97-106.

Clay CS and Medwin H. Acoustical Oceanography: Principles and Applications . New York: John Wiley and Sons, 1977.

Cloutier G, Qin Z. Shear rate dependence of normal, hypo-, and hyper-aggregating erythrocytes studied with power Doppler ultrasound. In: Lees S, Ferrari LA (Eds.). Acoustical Imaging. New York: Plenum Publishing Corporation, 1997a. pp. 291-6.

Cloutier G and Qin Z. Ultrasound backscattering from non-aggregating and aggregating erythrocytes-a review. Biorheology 1997b;34:443-470.

Cloutier G, Weng X, Roederer GO, Allard L, Tardif F and Beaulieu R. Differences in the erythrocyte aggregation level between veins and arteries of normolipidemic and hyperlipidemic individuals. Ultrasound Med. Biol. 1997;23:1383-1393.

Cloutier G, Zhao Qin, Durand L- and Beng Ghee Teh. Power Doppler ultrasound evaluation of the shear rate and shear stress dependences of red blood cell aggregation. Biomedical Engineering, IEEE Transactions on 1996;43:441-450.

de Kroon, M. G. M., Slager CJ, Gussenhoven WJ, Serruys PW, Roelandt, J. R. T. C. and Bom N. Cyclic changes of blood echogenicity in high-frequency ultrasound. Ultrasound Med. Biol. 1991;17:723-728.

Donath E, Kuzmin P, Krabi A and Voigt A. Electrokinetics of structured interfaces with polymer depletion — a theoretical study. Coll. Polym. Sci. 1993;271:930-939.

Epanechnikov VA. Non-parametric estimation of a multivariate probability density. Theory Probab. Appl. 1969;14:153-158.

Ernst E, Resch KL, Matrai A, Buhl M, Schilosser P and Paulsen HF. Impaired blood rheology: a risk factor after stroke?. J.Intern.Med. 1991;229:457-462.

Evans E, Berk D, Leung A and Mohandas N. Detachment of agglutinin-bonded red blood cells. II. Mechanical energies to separate large contact areas. Biophys. J. 1991;59:849-860.

Fatkin D, Loupas T, Jacobs N and Feneley MP. Quantification of blood echogenicity: Evaluation of a semiquantitative method of grading spontaneous echo contrast. Ultrasound Med.Biol. 1995;21:1191-1198.

Fatkin D, Loupas T, Low J and Feneley M. Inhibition of Red Cell Aggregation Prevents Spontaneous Echocardiographic Contrast Formation in Human Blood. Circulation 1997;96:889-896.

Foote KG. Speed of sound in Euphausia superba. J. Acoust. Soc. Am. 1990;87:1405-1408.

Fukuyo Y, Takano H, Chihara M, Matsuoka K. Red Tide Organisms in Japan. An Illustrated Taxonomic Guide . Tokyo: Uchida Rokakuho, Co., Ltd., 1990.

Gárate-Lizárraga I, López-Cortes DJ, Bustillos-Guzmán JJ and Hernández-Sandoval F. Blooms of Cochlodinium polykrikoides (Gymnodiniaceae) in the Gulf of California, Mexico. Rev. Biol. Trop. 2004;52(Suppl. 1):51-58.

Greenlaw CF. Acoustical estimation of zooplankton populations. Limnol. Oceanogr. 1979;24:226-242.

Greenlaw CF and Johnson RK. Physical and acoustical properties of zooplankton. J. Acoust. Soc. Am. 1982;72:1706-1710.

90

Greenlaw CF, Johnson RK and Pommeranz T. Volume scattering strength predictions for Antarctic krill. (Euphausia superba Dana). Meeresforsch. 1980;28:48-55.

Guillard RRL. Culture of phytoplankton for feeding marine invertebrates. In: Smith WL, Chanley MH eds. Culture of Marine Invertebrate Animals. New York: Plenum Press, 1975. pp. 26-60.

Guillard RRL and Ryther JH. Studies of marine planktonic diatoms. 1. Cyclotella nana Hustedt and Detonula confervacea (Cleve) Gran. Can. J. Microbiol. 1962;8:229-239.

Hahn R, Müller-Seydlitz PM, Jöckel KH, Hubert H and Heimburg P. Viscoelasticity and Red Blood Cell Aggregation in Patients with Coronary Heart Disease. Angiology 1989;40:914-920.

Hansen G. Cochlodinium polykrikoides, Protozoa(other), WoRMS Photogallery, http://www.marinespecies.org/photogallery.php?album=690&pic=25990, 2011.

Holliday DV and Pieper RE. Volume scattering strengths and zooplankton distributions at acoustic frequencies between 0.5 and 3 MHz. J. Acoust. Soc. Am. 1980;67:135-146.

Jiang X, Lonsdale DJ and Gobler CJ. Grazers and vitamins shape chain formation in a bloom-forming dinoflagellate, Cochlodinium polykrikoides. Oecologia. 2010;162:455-464.

Kamykowski D, Reed RE and Kirkpatrick GJ. Comparison of sinking velocity, swimming velocity, rotation and path characteristics among six marine dinoflagellate species. Marine Biology 1992;113:319-328.

Khan MM, Puniyani RR, Huilgol NG, Hussain MA and Ranade GG. Hemorheological profiles in cancer patients. Clin. Hemorheol. 1995;15:37-44.

Kils U. Preliminary data on volume, density and cross sectional area of Antarctic krill, Euphausia superba. Meeresforsch. 1979;27:207-209.

Kim E, Lee H, Na J, Choi JW and Kang D. 5-MHz acoustic-backscatter measurements of Cochlodinium polykrikoides blooms in Korean coastal waters. ICES Journal of Marine Science: Journal du Conseil 2010;67:1759-1765.

Kim HG. Cochlodinium polykrikoides blooms in Korean coastal waters and their mitigation. In: Reguera B, Blanco J, Fernandez ML, Wyatt T (Eds.). Harmful Algae, Xunta de Galicia and Intergovernmental Oceanographic Commission of UNESCO. Spain, 1998. pp. 227-8.

Kitamura H and Kawasaki S. Detection and clinical significance of red cell aggregation in the human subcutaneous vein using a high-frequency transducer (10 MHz): A preliminary report. Ultrasound Med. Biol. 1997;23:933-938.

Knisely MH. Intravascular erythrocyte aggregation (blood sludge). In: Hamilton FW, Dow P (Eds.). The Handbook of Physiology, section 2, Circulation Vol. III. Washington, D.C.: American Physiological Society, 1965. pp. 2249-98.

Koenig W and Ernst E. The possible role of hemorheology in atherothrombogenesis. Atherosclerosis 1992;94:93-107.

Køgeler JW, Falk-Petersen S, Kristensen Å, Pettersen F and Dalen J. Density- and sound speed contrasts in sub-Arctic zooplankton. Polar Biol. 1987;7:231-235.

Lavery AC, Wiebe PH, Stanton TK, Lawson GL, Benfield MC and Copley N. Determining dominant scatterers of sound in mixed zooplankton populations. J. Acoust. Soc. Am. 2007;122:3304-3326.

Lawson GL, Wiebe PH, Stanton TK and Ashjian CJ. Euphausiid distribution along the Western Antarctic Peninsula—Part A: Development of robust multi-frequency acoustic techniques to identify euphausiid aggregations and quantify euphausiid size, abundance, and biomass. Deep Sea Research Part II: Topical Studies in Oceanography 2008;55:412-431.

Le Devehat C, Vmeux M, Bondoux G and Khodababdehlou T. Red blood cell aggregation in diabetes mellitus. Int. Angiol. 1990;9:11-15.

Lee CK, Kim HC, Lee S-, Jung CS, Kim HG and Lim WA. Abundance of Harmful Algae, Cochlodinium polykrikoides, Gyrodinium impudicum and Gymnodinium catenatum in the Coastal Area of South Sea of Korea and Their Effects of Temperature, Salinity, Irradiance and Nutrient on the Growth in Culture. J. Korean Fish. Soc. 2001;34:536-544.

Lewitus AJ and Kana TM. Responses of estuarine phytoplankton to exogenous glucose: Stimulation versus inhibition of photosynthesis and respiration. Limnol. Oceanogr. 1994;39:182-189.

Li Y, Bok T, Yang J, Choi MJ and Paeng D. The Acute Effects of Smoking on the Cyclic Variations in Blood Echogenicity of Carotid Artery. Ultrasound Med.Biol. 2011;37:513-521.

Li W, van der Steen AFW, Lancee CT, Honkoop J, Gussenhoven EJ and Bom N. Temporal correlation of blood scattering signals in vivo from radiofrequency intravascular ultrasound. Ultrasound Med.Biol. 1996;22:583-590.

Machlup S. A Theoretical Model for Sound Scattering by Marine Crustaceans. J. Acoust. Soc. Am. 1952;24:290-293.

MacRury SM, Lennie SE, McColl P, Balendra R, MacCuish AC and Lowe GDO. Increased red cell aggregation in diabetes mellitus: Association with cardiovascular risk factors. Diabet. Med 1993;10:21-26.

Marañón E, Cermeño P, Rodríguez J, Zubkov MV and Harris RP. Scaling of phytoplankton photosynthesis and cell size in the ocean. Limnol. Oceanogr. 2007;52:2190-2198.

Margalef R. Hidrografia y fitoplancton de un area marina de la costa meridional de Puerto Rico. Inv. Pesq. 1961;18:76-78.

Matsuoka K and Fukuyo Y. Cochlodinium polykrikoides Margalef, WESTPAC/HAB, *http://dinos.anesc.u-tokyo.ac.jp/Jpeg/HABspecies/014cochl.jpg*, 2011.

Matsuoka K, Iwataki M and Kawami H. Morphology and taxonomy of chain-forming species of the genus Cochlodinium (Dinophyceae). Harmful Algae 2008;7:261-270.

Miller B and Heilmann L. Hemorheological parameters in patients with gynecologic malignancies. Gynecol.Oncol. 1989;33:177-181.

Morris DJ, Watkins JL, Ricketts C, Buchholz F and Priddle J. An assessment of the merits of length and weight measurements of Antarctic krill Euphausia superba. Br. Antarct. Surv. Bull. 1988;79:27-50.

Mulholland M, Morse R, Boneillo G, Bernhardt P, Filippino K, Procise L, Blanco-Garcia J, Marshall H, Egerton T, Hunley W, Moore K, Berry D and Gobler C. Understanding Causes and Impacts of the Dinoflagellate, Cochlodinium polykrikoides, Blooms in the Chesapeake Bay. Estuaries and Coasts 2009;32:734-747.

Nam K, Paeng D and Choi MJ. Ultrasonic backscatter from rat blood in aggregating media under in vitro rotational flow. Ultrasonics, Ferroelectrics and Frequency Control, IEEE Transactions on 2009;56:270-279.

Nam K, Paeng D, Choi MJ and Shung KK. Ultrasonic Observation of Blood Disturbance in a Stenosed Tube: Effects of Flow Acceleration and Turbulence Downstream. Ultrasound Med.Biol. 2008;34:114-122.

Neumann FJ, Katus HA, Hoberg E, Roebruck P, Braun M, Haupt HM, Tillmanns H and Kübler W. Increased plasma viscosity and erythrocyte aggregation: Indicators of an unfavorable clinical outcome in patients with unstable angina pectoris. Br. Heart J. 1991;66:425-430.

Nichols WW and O'Rourke MF. McDonald's Blood Flow in Arteries: Theoretical, Experimental and Clinical Principles 5th. New York: Hodder Arnold, Oxford University Press, 2005.

Oh SJ, Yoon YH, Kim D, Shimasaki Y, Oshima Y and Honjo T. Effects of Light Quantity and Quality on the Growth of the Harmful Dinoflagellate, Cochlodinium polykrikoides Margalef (Dinophyceae). Algae 2006;21:311-316.

Paeng D, Chiao RY and Shung KK. Echogenicity variations from porcine blood I: the "bright collapsing ring" under pulsatile flow. Ultrasound Med.Biol. 2004a;30:45-55.

Paeng D, Chiao RY and Shung KK. Echogenicity variations from porcine blood II: the "bright ring" under oscillatory flow. Ultrasound Med.Biol. 2004b;30:815-825.

Paeng D, Choi MJ and Shung KK. Investigation of blood under pulsatile flow using ultrasound imaging. Int. Congr. Ser. 2004c;1274:99-108.

Paeng D, Nam K and Shung KK. Cyclic and radial variation of the echogenicity of blood in human carotid arteries observed by harmonic imaging. Ultrasound Med. Biol. 2010;36:1118-1124.

Paeng D and Shung KK. Cyclic and radial variation of the Doppler power from porcine whole blood. Ultrasonics, Ferroelectrics and Frequency Control, IEEE Transactions on 2003;50:614-622.

Palmer DR. Rayleigh scattering from nonspherical particles. J. Acoust. Soc. Am. 1996;99:1901-1912.

Poggi M, Palareti G, Biagi R, Legnani C, Parenti M, Babini AC, Baraldi L and Coccheri S. Prolonged very low calorie diet in highly obese subjects reduces plasma viscosity and red cell aggregation but not fibrinogen. Int. J. Obes. Relat. Metab. Disord. 1994;18:490-496.

Rabhi YA, Fabbro-Peray P, Dauzat M, Montesinos P, Oliva-Lauraire MC, Lopez FM, Quéré I, Gris JC, Brun JF and Pourcelot L. Towards a quantitative in vivo evaluation of venous blood echogenicity: image processing versus subjective assessment. Clin. Hemorheol. Microcirc. 2002;27:27-41.

Rampling MW, Meiselman HJ, Neu B and Baskurt OK. Influence of cell-specific factors on red blood cell aggregation. Biorheology 2004;41:91-112.

Rayleigh JWS. Investigation of the disturbance produced by a spherical obstacle on the waves of sound. Proc. Lond. Math. Soc. 1972;4:253-283.

Rayleigh JWS. On the passage of waves through apertures in plane screens and allied problems. Phil. Mag. 1897;43:259-272.

Razavian SM, Atger V, Giral P, Cambillau M, Del-Pino M, Simon AC, Moatti N, Levenson J and the PCVMETRA Group. Influence of HDL subfractions on erythrocyte aggregation in hypercholesterolemic men. Arterioscler. Thromb. Vasc. Biol. 1994;14:361-366.

Razavian SM, Del Pino M, Simon A and Levenson J. Increase in erythrocyte disaggregation

shear stress in hypertension. Hypertension 1992;20:247-252.

Razavian SM, Levenson J, Peronneau P and Simon A. Quantification of erythrocyte

aggregation by blood echogenicity: a preliminary study. J. Cardiovasc. Surg.

1995a;36:375-377.

Razavian SM, Linhart A, Massonneau M, Simon A and Levenson J. Quantification of

erythrocyte aggregation by blood echogenicity: In-vitro and in-vivo measurements.

Biorheology 1995b;32:215-216.

Resch KL, Ernst E, Matrai A, Buhl M, Schlosser P and Paulsen HF. Can Rheologic Variables

be of Prognostic Relevance in Arteriosclerotic Diseases?. Angiology

1991;42:963-970.

Reynolds AJ. Turbulent Flows in Engineering . New York: John Wiley & Sons, 1974.

Roberts PLD and Jaffe JS. Classification of live, untethered zooplankton from observations of

multiple-angle acoustic scatter. J. Acoust. Soc. Am. 2008;124:796-802.

Romer AS and Parsons TS. The Vertebrate Body 6th. Philadelphia: Holt-Saunders

International, 1977.

Rosenblatt M. Remarks on some nonparametric estimates of a density function. Ann. Math. Statist. 1956;27:832-837.

Savérya D and Cloutier G. High-frequency ultrasound backscattering by blood: Analytical and semianalytical models of the erythrocyte cross section. J. Acoust. Soc. Am. 2007;121:3963-3971.

Schlichting H. Boundary-layer theory 6th. New York: McGraw-Hill, 1968.

Schmid-Schobein H and Volger E. Red-cell aggregation and red-cell deformability in diabetes. Diametes 1976;25:897-902.

Sharma K, Puniyani RR, Bhat SV, Advani SH, Hegde U and Rao S. Blood viscosity parameter correlation with types of leukemia. Physiol. Chem. Phys. Med. NMR 1992;24:159-164.

Shehada REN, Cobbold RSC and Mo LY-. Aggregation effects in whole blood: influence of time and shear rate measured using ultrasound. Biorheology 1994;31:115-135.

Shung KK, Yuan YW, Fei DY and Tarbell JM. Effect of flow disturbance on ultrasonic backscatter from blood. J. Acoust. Soc. Am. 1984;75:1265-1272.

Shung KK and Cloutier G. The effects of hematocrit shear rate and turbulence on ultrasonic Doppler spectrum from blood. IEEE Trans. Biomed. Eng. 1992;39:462-469.

Shung KK, Sigelmann RA and Reid JM. Angular Dependence of Scattering of Ultrasound from Blood. Biomedical Engineering, IEEE Transactions on 1977;BME-24:325-331.

Shung KK, Sigelmann RA and Reid JM. Scattering of Ultrasound by Blood. Biomedical Engineering, IEEE Transactions on 1976;BME-23:460-467.

Sigel B, Machi J, Beitler JC and Justin JR. Red cell aggregation as a cause of blood-flow echogenicity. Radiology 1983;148:799-802.

Sigel B, Machi J, Beitler JC, Justin JR and Coelho JC. Variable ultrasound echogenicity in flowing blood. Science 1982;218:1321-1323.

Silva ES. Cochlodinium heterolabatum n.sp.: Structure and some cytophysiological aspects. J. Protozool. 1967;14:745-754.

Stanton TK. Sound scattering by cylinders of finite length. III. Deformed cylinders. J. Acoust. Soc. Am. 1989;86:691-705.

Stanton TK. Sound scattering by cylinders of finite length. I. Fluid cylinders. J. Acoust. Soc. Am. 1988;83:55-63.

Stanton TK, Chu D and Wiebe PH. Sound scattering by several zooplankton groups. II. Scattering models. J. Acoust. Soc. Am. 1998;103:236-253.

Stanton TK, Chu D, Wiebe PH and Clay CS. Average echoes from randomly oriented random-length finite cylinders: Zooplankton models. J. Acoust. Soc. Am. 1993;94:3463-3472.

Stanton TK, Chu D, Wiebe PH, Martin LV and Eastwood RL. Sound scattering by several zooplankton groups. I. Experimental determination of dominant scattering mechanisms. J. Acoust. Soc. Am. 1998;103:225-235.

Stanton TK, Wiebe PH, Chu D, Benfield MC, Scanlon L, Martin L and Eastwood RL. On acoustic estimates of zooplankton biomass. ICES Journal of Marine Science: Journal du Conseil 1994;51:505-512.

Steidinger KA, Tangen K. Dinoflagellates. In: Tomas CR (Ed.). Identifying Marine Diatoms and Dinoflagellates. New York: Academic Press, 1996. pp. 387-598.

Suh Y-, Kim J- and Kim H-. Relationship between Sea Surface Temperature derived from NOAA Satellites and Cochlodinium polykrikoides Red Tide occurrence in Korean Coastal Waters. J. Kor. Environ. Sci. Soc. 2000;9:215-221.

Tanahashi N, Fukuuchi Y, Tomita M, Matsuoka S and Takeda H. Erythrocyte aggregability in patients with cerebral infaction with special reference to diabetes mellitus. Clin. Hemorheol. 1993;13:253-259.

Tanahashi N, Gotoh F, Tomita M, Shinohara T, Terayama Y, Mihara B, Ohta K and Nara M. Enhanced erythrocyte aggregability in occlusive cerebrovascular disease. Stroke 1989;20:1202-1207.

Taylor FJR, Fukuyo Y, Larsen J. Taxonomy of harmful dinoflagellates. In: Hallegraeff GM, Anderson DM, Cembella AD (Eds.). Manual on Harmful Marine Microalgae, IOC Manuals and Guides No. 33. France: UNESCO, 1995. pp. 283-317.

van der Heiden, Maurits S., de Kroon, Machteld G. M., Bom N and Borst C. Ultrasound backscatter at 30 MHz from human blood: Influence of rouleau size affected by blood modification and shear rate. Ultrasound Med.Biol. 1995;21:817-826.

van Oss C, Atger V and Coakley W. Depletion flocculation and depletion stabilization of erythrocytes. Cell Biochemistry and Biophysics 1990;17:1-10.

Volger E. Effect of metabolic control and concomitant diseases upon the rheology of blood in different states of diabetic retinopathy. Horm. Metabol. Res. Suppl. 1981;11:104-107.

Wang S and Shung KK. In vivo measurements of ultrasonic backscattering in blood. Ultrasonics, Ferroelectrics and Frequency Control, IEEE Transactions on 2001;48:425-431.

Warren JD and Smith JN. Density and sound speed of two gelatinous zooplankton: Ctenophore (Mnemiopsis leidyi) and lion's mane jellyfish (Cyanea capillata). J. Acoust. Soc. Am. 2007;122:574-580.

Watkins JL. Variations in the size of Antarctic krill, Euphausia superba. Mar. Ecol. Prog. Ser. 1986;31:67-73.

Wiebe PH, Mountain DG, Stanton TK, Greene CH, Lough G, Kaartvedt S, Dawson J and Copley N. Acoustical study of the spatial distribution of plankton on Georges Bank and the relationship between volume backscattering strength and the taxonomic composition of the plankton. Deep Sea Research Part II: Topical Studies in Oceanography 1996;43:1971-2001.

Wikipedia. Radial artery, *http://en.wikipedia.org/wiki/Radial_artery*, 2011.

Wikipedia. Radial artery image, *http://commons.wikimedia.org/wiki/File:Gray1237.png*, 2011.

Womersley JR. Method for the calculation of velocity, rate of flow and viscous drag in arteries when the pressure gradient is known. J. Physiol. 1955;127:553-563.

Yamasaki Y, Nagasoe S, Matsubara T, Shikata T, Shimasaki Y, Oshima Y and Honjo T. Growth inhibition and formation of morphologically abnormal cells of Akashiwo

sanguinea (Hirasaka) G. Hansen et Moestrup by cell contact with Cochlodinium polykrikoides Margalef. Marine Biology 2007;152:157-163.

Yoo YD, Jeong HJ, Shim JH, Park JY, Lee KJ, Yih W, Kweon HK, Pae SJ and Park JG. Outbreak of Red Tides in the Coastal Waters off the Southern Saemankeum areas, Jeonbuk, Korea; 1. Temporal and Spatial Variations in the Phytoplankton Community in the Summer-Fall of 1999. J. Kor. Soc. Oceanogr. 1999;7:129-139.

Yuan YW and Shung KK. Ultrasonic backscatter from flowing whole blood. I: Dependence on shear rate and hematocrit. J. Acoust. Soc. Am. 1988;84:52-58.

Yuan YW and Shung KK. Echoicity of whole blood. J. Ultrasound Med. 1989;8:425-434.

Yuan YW and Shung KK. Ultrasonic backscatter from flowing whole blood. II: Dependence on frequency and fibrinogen concentration. J. Acoust. Soc. Am. 1988;84:1195-1200.

Yuki K, Yoshimatsu S. Two fish-killing species of Cochlodinium from Harima-Nada, Seto Inland Sea, Japan. In: Okaichi T, Anderson D, Nemoto T (Eds.). Red Tides: Biology, Environmental Science, and Toxicology. New York: Elsevier, 1989. pp. 451-4.

ACKNOWLEDGEMENT (in KOREAN)